Australian Government
Department of Defence
Defence Science and
Technology Organisation

# The Aerosol Models in MODTRAN: Incorporating Selected Measurements from Northern Australia

*S. B. Carr*

**Intelligence, Surveillance and Reconnaissance Division**
Defence Science and Technology Organisation

DSTO-TR-1803

## ABSTRACT

The aerosol models in MODTRAN are discussed. The focus in this report is on the boundary layer aerosol. The second part of the report outlines the major results of aircraft measurements of atmospheric aerosol obtained around Jabiru, N.T., in June and September 2003. These measurements are used to obtain theoretical multimode size distribution functions. The chemistry composition measurements are used with selected results from the literature to derive spectral refractive indices for the biomass burning smoke aerosol. These results are then used in Mie scattering calculations of the aerosol extinction and scattering coefficients. The attenuation coefficients are then incorporated into MODTRAN and compared with the default aerosol models. Finally the Jabiru aerosol is used in calculations of atmospheric transmission over a series of paths: horizontal, vertical and slant paths. The major result is that the aerosol concentration is quite low giving rise to large visibilities and hence the effect of the atmospheric aerosol on the transmission of radiation over visible and thermal wavebands is small for paths less than around 30 km.

## RELEASE LIMITATION

*Approved for public release*

*Published by*

*DSTO Defence Science and Technology Organisation*
*PO Box 1500*
*Edinburgh South Australia 5111  Australia*

*Telephone:  (08) 8259 5555*
*Fax:  (08) 8259 6567*


*AR-013-545*
*December 2005*

**APPROVED FOR PUBLIC RELEASE**

# The Aerosol Models in MODTRAN: Incorporating Selected Measurements from Northern Australia

## Executive Summary

The long range research (LRR) task 04/175 EO Systems and Environment Modelling was established to allow DSTO to improve its electro-optical (EO) modelling capability. This work is a key research activity (KRA) in the information sciences laboratory LRR program (FRAC R2) aimed at contributing to research topic three - situation awareness. The results presented in this report are part of the key research output for the year 2005/2006. The majority of EO systems are imaging and are used to offer surveillance, reconnaissance and intelligence gathering capabilities to military and civilian agencies. They are also used as a component of a weapon system primarily to assist with targeting an adversary. In secondary roles they can be used for vehicle pilotage and non combat related activities such as search and rescue. The condition of the atmosphere is a significant factor that impacts on the performance of EO systems.

This report focuses on incorporating atmospheric aerosol measurements made in the North of Australia into the atmospheric propagation model called MODTRAN (MODerate spectral atmospheric TRANsmission). This model is a US model developed for Northern hemisphere conditions. It is used to take account of the effect the atmosphere has on radiation propagation between the target and a sensor. A brief outline of these measurements is included in this report but the detailed analysis is presented in the DSTO research report DSTO-RR-0298.

The measurements are a combination of aircraft and ground measurements centred on Jabiru in the Northern Territory, Australia. This environment is typical of a Northern Australian dry season climate. Atmospheric transmission calculations have been performed using the Jabiru aerosol measurements. These have been compared with two default aerosol models in MODTRAN: the rural and maritime models. Calculations of atmospheric transmission are made over a series of paths: horizontal, vertical and slant paths. The atmosphere around Jabiru is very clean, despite the continual presence of biomass burning activity during the dry season. The burning occurs over a large region (the top end) and the short duration of the fires results in low levels of smoke aerosol aloft. The exception is viewing directly through a smoke plume or fire front. This translates to large visibilities of the order of 100 kilometres (km) or more. It is only over very long slant paths that the impact of aerosol attenuation starts to impact on visible and mid wave infrared (3-5 micrometres (μm)) wavebands in this region.

The results of this report give DSTO the ability to more accurately assess the use of aerosol models in MODTRAN. This will allow for a more precise use of the model in studies on EO sensor performance in the tropical North of Australia. A quantitative assessment of the aerosol models in MODTRAN allows DSTO to provide more robust advice to the ADF and civilian agencies, as required, on the performance of EO sensors.

# Authors

**Dr Stephen Carr**
Intelligence, Surveillance and Reconnaissance Div.

*Before joining DSTO as a Research Scientist in early 1998, Dr Carr completed an Honours Degree in 1991 and a PhD in 1996 both in Theoretical Physics at The Flinders University of South Australia. Shortly after joining the Weapons Systems Division he became Task Manager of the Infra Red Search and Track (IRST) task for the Navy which he worked on from 1998 through to the end of 2001. During his time in WSD he was involved with work on anti-personnel land mine alternatives and land based IRST as part of ground based air defence studies. Since joining ISRD in 2001 as a Senior Research Scientist he has been Task Manager for LRR 01/205 Atmospheric Aerosol Research and LRR 04/175 EO Systems and Environment Modelling.*

# Contents

# 1. Introduction

The aerosol models that form part of the atmospheric propagation code MODTRAN (MODerate spectral atmospheric TRANsmission) [3] are summarised. The current version of MODTRAN is 5 [4]. The aerosol models have remained unchanged since version 3.7. There is a new capability in MODTRAN 5 to model a boundary layer aerosol. The extinction coefficient is derived assuming the underlying aerosol particle number size distribution is governed by a power law. This and a related modification will not be addressed in this report. In this report we shall refer to the particle number size distribution simply as the size distribution.

The bulk of the report outlines the incorporation of some measurements of the biomass burning aerosol size distributions and refractive indices into MODTRAN 4 version 1 release 1 (v1r1) [5]. These measurements were obtained around Jabiru, Northern Territory (N.T.) Australia during June and September 2003. Data was collected on the chemical, microphysical and optical properties of the regional aerosol [2]. Unless otherwise stated, when we refer to MODTRAN throughout the remainder of this report we mean MODTRAN 4 v1 r1.

The biomass burning smoke aerosol is modelled assuming the particles are spherical and Mie scattering theory is used to calculate the extinction and absorption coefficients. The size distribution data from the aircraft measurements are used in the calculations. A composite spectral refractive index for the biomass smoke is derived from data obtained from the literature.

The spectral attenuation coefficients are then combined with the boundary layer aerosol vertical scale factor in MODTRAN. Calculations are made of the atmospheric transmission for a range of paths through the atmosphere. The results of using the Jabiru aerosol in transmission calculations are compared with the rural and maritime aerosol models of MODTRAN.

## 1.1 Background

In the past, the LOWTRAN (LOW spectral atmospheric TRANsmission) [6] model has been assessed to determine its suitability for use in predicting atmospheric transmission of electromagnetic radiation (ultraviolet (UV), visible, infrared (IR)) for Australian conditions [7, 8]. The focus of the majority of those studies was on IR atmospheric transmission measurements for temperate and tropical environments allowing for the partial validation of LOWTRAN. No major attempt was made to characterise the aerosol. Measurements were made at one end of the transmission path (the radiometer end) [9, 10]. Aerosol size distribution curves were obtained. The elemental composition of the aerosol particles was determined using x-ray fluorescence. These results were not reported on in detail. The measurements were limited to one location on the ground and did not provide an insight into how the aerosol is distributed spatially throughout the boundary layer and the free troposphere. The measurements built upon some earlier theoretical studies that made use of Mie calculations of aerosol scattering coefficients [11] and a literature review [12]. The work that has been undertaken in the past forms a backdrop to the results presented in this report.

With the advent of modern day computers and sophisticated aerosol measuring equipment, the results presented in this report represent a quantum leap ahead in our capability to characterise atmospheric aerosol. They represent a further step forward taken by the DSTO (and its predecessors) in the understanding of the effect the atmosphere (in particular the atmospheric aerosol) has on the transmission of radiation.

### 1.2 An Alternative Atmospheric Model

The focus of this report is on the atmospheric model MODTRAN. An alternative model to MODTRAN is MOSART (Moderate Spectral Atmospheric Radiance and Transmittance) [13]. The details of this model are beyond the scope of this report. MOSART offers some improvements over MODTRAN in the modelling of aerosol. In the future, consideration should be given to using MOSART and to determining under what circumstances it is more appropriate to make use of MOSART.

MOSART more accurately calculates the height of the tropopause (primary) and stratopause as a function of the atmospheric conditions. This will result in a more accurate representation of the vertical profile of the aerosol particle number concentration. The former shall be referred to as the vertical aerosol profile or just the vertical profile in the remainder of the report. The correct value for the Rayleigh scattering coefficient for air is calculated by MOSART for each model atmosphere. MODTRAN assumes a constant value, which is used in calculations of surface meteorological range and will result in error. The Mie scattering code that accompanies MODTRAN is based on the assumption of an internally mixed aerosol particle. The Mie code used by MOSART is more general and assumes the particle can be represented by a core which is a mixture of two materials surrounded by a spherical coating. This provides the user with greater flexibility to model a range of aerosol mixtures. The Mie code in MODTRAN includes a larger number of modelled size distribution functions. In particular the options of the sums of two and three lognormal size distribution functions are available to the user.

Imagery Systems Branch located within Intelligence Surveillance and Reconnaissance Division (ISRD) is collaborating with Dr Bill Cornette of the US Air Force; the developer of the MOSART code. There are plans to incorporate some of the aerosol measurements referred to in this report into MOSART. This work is ongoing and may be reported on at a later date.

## 2. The Aerosol Models in MODTRAN

### 2.1 Overview of MODTRAN

The following information is taken from The MODTRAN 2/3 and LOWTRAN 7 Model report [3]. The MODTRAN model calculates atmospheric transmittance, atmospheric background radiance, single-scattered solar and lunar radiance, direct solar and lunar irradiance and multiple-scattered solar and thermal radiance. The spectral resolution of MODTRAN is $\nu$ = 2 $cm^{-1}$ FWHM (full-width half maximum) in averaged steps of 1 $cm^{-1}$, where $\nu$ is wavenumber given in units of inverse centimetres. Wavenumber is defined as $\nu=1/\lambda$, where

$\lambda$ is wavelength. MODTRAN 5 [4] extends the spectral resolution to 0.1 $cm^{-1}$. The effects of molecular continuum-type absorption; molecular scattering, aerosol and hydrometeor absorption and scattering are all included. MODTRAN also includes a molecular band model to account for molecular absorption.

Representative atmospheric aerosol, cloud and rain models are provided within the code with options to replace them with user-modelled or measured values. Spherical refraction and earth curvature (ray bending) are considered in the calculation of atmospheric slant path and attenuation amounts along the path.

Six reference atmospheres, each defined by temperature, pressure, density, and mixing ratios for $H_2O$, $O_3$, $CH_4$, $CO$ and $N_2O$, all as a function of altitude allow a wide range of climatological choices. The $CO_2$ mixing ratio is a variable that can be entered by the user. For the results presented in this report it is taken to be 365 ppmv (parts per million by volume). Atmospheric molecular constituent profiles containing separate molecular profiles (0-120 kilometres (km)) for thirteen minor and trace gases are available. Aerosol models are then combined with these reference atmospheres as required. The atmospheres are taken from the Northern hemisphere and are listed in Table 1.

*Table 1: The six reference atmospheres of MODTRAN referenced to Northern Hemisphere locations and seasons (as specified by the month).*

| Model Atmosphere | Location | Time of the Year |
|---|---|---|
| Tropical | 15 N | Annual Average |
| Mid-Latitude Summer | 45 N | July |
| Mid-Latitude Winter | 45 N | January |
| Sub-Artic Summer | 60 N | July |
| Sub-Artic Winter | 60 N | January |
| US Standard | US | 1976 |

In recent versions of MODTRAN [4, 5], there has been an improvement in the treatment of multiple scattering and an increase in the spectral resolution. The aerosol models underwent a major enhancement in version 3.7. The user is now able to move the aerosol models to arbitrary regions and scale, compress and stretch the vertical profiles as required. The details about the molecular constituents (gases) and atmospheric radiance calculations of MODTRAN are not investigated in this report.

The aerosol models in MODTRAN are defined by regions that contain typical aerosol sources. The sources are representative of rural, urban, desert and maritime environments. For higher altitudes, the aerosols are assumed to be the same whether over land or sea. For the purpose of assigning aerosol models, the atmosphere is dived into vertical regions: the boundary layer (0 - 2 km), the free troposphere (background troposphere) (2 - 10 km), the lower stratosphere (10 - 30 km) and the upper atmosphere (30 - 100 km). This is only provided as a guide. In MODTRAN 3.7 the user is provided with the option to shift the aerosol models around and to alter the height of the tropopause for example. This enables the vertical aerosol profile to be

more accurately modelled. In this report we will focus on analysing the aerosol models from the boundary layer.

The modelling of aerosols in MODTRAN has two key functions

1. the accurate representation of the chemical and physical properties of the aerosol particles and from this to account for their optical properties e.g. refractive index , and
2. the accurate representation of the vertical distribution of the aerosol particle number concentration in the atmosphere.

## 2.2 Boundary Layer Aerosols

### 2.2.1 The Models of Shettle and Fenn

The majority of the boundary layer aerosol models in MODTRAN were developed by Shettle and Fenn [14]. The models were constructed to represent the basic aerosol types on a regional basis: urban, rural, maritime and tropospheric (this is not a boundary layer aerosol). For very clear conditions it is recommended that the tropospheric aerosol model be used in the boundary layer. A literature survey was undertaken, and a large amount of information was collected on the chemistry, physics and derived optical properties of the basic aerosol components, for each of these regions.

The models of Shettle and Fenn are built upon more fundamental components. The main components being: water soluble, dust like, soot, sea salt and water (entering through the effect of relative humidity (RH) changes on the aerosol particles size (radius) and refractive index). From these fundamental components a composite or average aerosol is constructed for each of the regions mentioned above. This type of aerosol is called internally mixed. The average aerosol particle is a homogeneous mixture of each of the basic chemical components. The urban aerosol model has a component that is rural, but weighted (by volume) with additional species representing anthropogenic aerosol sources. The maritime aerosol has a rural component corresponding to aerosol of a continental origin and a sea salt component consistent with aerosol with oceanic origins. Each regional aerosol is represented by a log normal physical size distribution or the sum of two log normal functions. This represents the distribution of particle numbers as a function of size (radius in this case). In the majority of cases aerosol particles belong to one of the following modes: the fine particle mode (nucleation, Aitken and accumulation modes) and the coarse particle mode. The boundary layer aerosol models do not have a nucleation mode. The Aitken mode, representing fresh smoke particles for example, has been ignored. Shettle and Fenn state that the effect of this mode is small on the optical properties of the aerosol. These models are used in calculations of atmospheric transmission and path radiance within the atmosphere, so this is well justified.

The majority of aerosol species and therefore internally mixed aerosol particles are hygroscopic. Shettle and Fenn model the growth in the size of aerosol particles and changes in particle refractive index as a function of relative humidity. This is done in such a way, that when used in MODTRAN, the models give an accurate representation of the atmospheric aerosol under ambient conditions.

It is worth reiterating what is stated in the report by Shettle and Fenn. "While these aerosol models were developed to be representative as possible of different atmospheric conditions, the following point should be kept in mind when using any such model: Given the natural variability of the atmospheric aerosols almost any aerosol model is supported by some measurements and no model (or set of models) will be consistent with all measurements". They go on to state elsewhere in the report 'Yet the simple question: "Which model (meaning which aerosol model) should be used for what location and weather situation?" is difficult to answer precisely.'

#### *2.2.1.1 Rural Model*

This model is intended to represent regions of the atmosphere not impacted upon by urban or industrial processes. It is assumed to be composed of 70% water soluble material (ammonium, calcium sulphate and organic compounds) and 30% dust like aerosol.

The dust like aerosol makes up the majority of the coarse mode. Ideally the fine and coarse modes should be treated independently of each other. The relevant amounts of water soluble and dust like material included in the average aerosol particles for the two modes will be different. The relative growth in particle diameter and the change in refractive index as a function of relative humidity will also differ for the two modes. In the models of Shettle and Fenn no distinction is made between particle modes in terms of the chemical composition of the aerosols. A single composite particle is used. They state that this does not introduce any appreciable error. It was done primarily to reduce the number of Mie calculations necessary to determine the refractive index which is calculated as a function of RH. This is no longer an issue with the computational speed of modern computers (note the work of Shettle and Fenn dates back before 1980).

#### *2.2.1.2 Urban Model*

The urban aerosol is the rural aerosol modified by the presence of aerosol from combustion and industrial sources. To account for these additional aerosol sources the urban aerosol is taken to be a mixture of the rural aerosol (80%) with carbonaceous aerosol (20%).

The size distribution of the elemental carbon aerosol is assumed to be the same as both components of the rural model. The refractive index of the elemental carbon aerosol was determined from data obtained from a survey of the refractive index of carbonaceous materials.

#### *2.2.1.3 Maritime Model*

This model aerosol is composed of a sea-salt component and a continental component, which is the rural aerosol with the exception that the larger particles (dust like) are eliminated. This is justified on the grounds that the larger particles will fall out of the atmosphere as a result of gravitational settling. This occurs over periods of hours and days as the air mass moves from land across the ocean. The user is able to adjust the relative amounts of the oceanic and continental types of aerosol to take account of changes between open ocean and littoral environments.

The model does not account for fresh sea spray that exists in the lower altitudes above the sea surface (10 - 20 metres) and which is strongly dependent on wind speed. Maritime aerosol models are available in MODTRAN that model the near sea surface aerosol. In place of MODTRAN purpose built models such as IRBLEM (Infrared Boundary Layer Effects Model) can be used. This model is used to study IR radiation propagation through the atmosphere in the near sea surface layer.

#### *2.2.1.4 The Size Distribution Function*

The size distributions of these aerosol models are represented by one or the sum of two lognormal distribution functions. They have the following form

$$n(r) = \frac{dN(r)}{dr} = \sum_{i=1}^{2} \left( \frac{N_i}{\ln(10) r \sigma_i \sqrt{2\pi}} \right) \exp\left[ - \frac{(\log r - \log r_i)^2}{2{\sigma_i}^2} \right]$$

where $N(r)$ is the cumulative number density of particles of radius r; $\sigma$ is the standard deviation (note it is common to define the log normal size distribution in terms of the geometric standard deviation (GSD), which is often denoted by sigma as well); $r_i$ is the mode radius and $N_i$ is the number density with $r_i$. To avoid confusion in this report we shall use $\xi$ to symbolise the geometric standard deviation. The standard deviation and GSD are related by $\sigma = \log \xi$.

Tables and plots of important aerosol parameters are given in the report by Shettle and Fenn. This includes the individual component refractive indices versus wavelength, the number and volume size distribution parameters for each aerosol model and the volume weighted refractive indices as a function of wavelength and RH.

#### *2.2.1.5 Vertical Distribution in the Lower Atmosphere*

In the boundary layer, the shape of the size distribution and the chemical composition of the average aerosol particles are assumed to be invariant with altitude. The total number of aerosol particles varies as a function of altitude whilst the relative particle numbers between the different aerosol modes remains constant.

The variation in the number concentration is modelled differently depending on the surface meteorological range (VIS). In this report and in MODTRAN VIS refers to the surface meteorological range and not the observer visibility. They are approximately related by the following relationship

$$V_{obs} \approx VIS \,/ \left(1.3 \pm 0.3\right)$$

where $V_{obs}$ is the observer visibility. For hazy conditions (VIS = 2 to 10 km) the boundary layer aerosol extinction coefficient is assumed to be independent of height up to 1 km with a

pronounced decrease above that height. For VIS from 23 to 50 km (clear to very clear conditions) the vertical distribution of concentration is taken to be exponential.

Above the boundary layer, the aerosol characteristics become less sensitive to weather and geography. At these altitudes, changes are more a result of seasonal variations. The default vertical profiles of aerosol scaling factors (Section 2.4) are displayed in Figure 1.

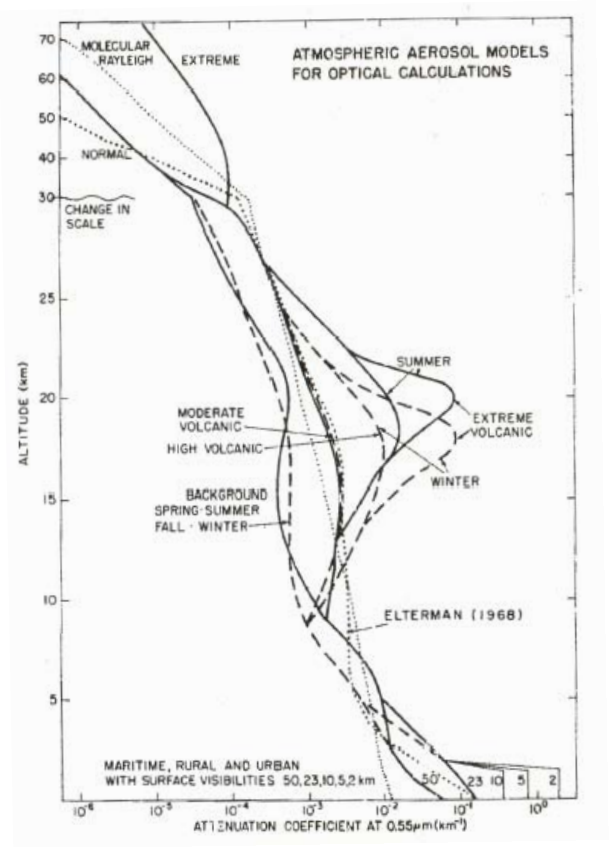


*Figure 1: The default vertical profiles of aerosol scaling factors from 0 to 70 km (reproduced here from a second report of Shettle and Fenn [15]).*

The flexible aerosol scheme was introduced in MODTRAN 3.7. The boundary layer aerosol models are no longer fixed to specific regions and can be translated, scaled, stretch or compressed.

### 2.2.2 Other Boundary Layer Aerosol Models

The Desert (wind dependent) aerosol model is representative of arid and semi arid regions. The desert aerosol model used is the tentative (United States) Air Force Geophysics Laboratory (AFGL) desert aerosol model referred to in The MODTRAN 2/3 and LOWTRAN 7 Model report.

Two types of desert aerosol models are used; a background desert model and a desert dust storm aerosol model. The background model is representative of aerosol that has been in the atmosphere for days or weeks and perhaps has been transported large distances on intercontinental winds. The main difference between the two models is the large number of particles around 10 μm in diameter in the dust storm model. This number is dependent on strong surface winds and represents an extreme situation. The parameters of the desert aerosol size distribution are primarily obtained from measurements undertaken in the Sahara Desert. The chemical composition of the desert aerosol is discussed in more detail in The MODTRAN 2/3 and LOWTRAN 7 Manual.

The Navy Aerosol Model (NAM) is an improvement over the maritime model of Shettle and Fenn. It includes the effects of wind speed. The other major difference is that NAM has three size modes representing three distinct populations of aerosol particles. The smallest component is a continental aerosol and is considered to be background. The second component consists of maritime aerosol that is dependent on the wind speed over the past 24 hours. Therefore it is representative of sea salt based particles that do not or have not fallen out of the atmosphere rapidly. The third component is fresh aerosol, the magnitude of which is dependent on current wind speed. The model takes into account RH changes in the atmosphere; in terms of the hygroscopic growth in the diameter of sea-salt particles and in the resultant changes in their refractive index. The NAM model requires the addition of three input parameters: ICSTL, indicating the degree of continental influence, WHH, the average wind speed over the past day and WSS the current wind speed.

The addition of the Navy Oceanic Vertical Aerosol Model (NOVAM) to MODTRAN provides greater flexibility to the user to model near sea surface aerosol. It is an upgrade to the NAM model already included in MODTRAN. Unlike NAM, NOVAM is provided as a standalone code which needs to be compiled and run producing output files needed by MODTRAN. The details of NOVAM are not discussed. The interested reader is referred to the NOVAM report [16].

## 2.3 Non Boundary Layer Models

The tropospheric aerosol model is used to represent the atmospheric aerosol above the boundary layer and below the tropopause. The aerosol particles are assumed to have the same composition as the rural aerosol model. As with the Maritime model the larger size particles are eliminated (course mode) from the model. Particles above the boundary layer have a longer residence time and the larger particles will settle out under gravity. This model takes into account changes in aerosol properties (diameter and refractive index) as a function of ambient relative humidity.

There is also a fog model. The remainder of the aerosol models in MODTRAN are for altitudes above the tropopause. These include a background stratospheric aerosol model, volcanic aerosol models and an upper atmosphere aerosol model. These models will not be discussed in this report. Details about them can be found in The MODTRAN 2/3 and LOWTRAN 7 Models report [3].

## 2.4 Aerosol Attenuation Coefficients and User Defined Aerosol Spectral Parameters

In MODTRAN, aerosol particles are treated as spheres and Mie scattering theory [17, 18] is used to calculate extinction and scattering efficiencies (or cross sections). The cross section for radiation scattering from a sphere is a function of the particle size and complex refractive index. The imaginary part accounts for absorption of some of the incident electromagnetic (EM) wave inside the sphere. The real part accounts for scattering of the incident wave, which in general is the dominant component of extinction. The exception is for aerosol particles with a significant fraction of elemental carbon.

The cross section is a function of the particle size and wavelength, $\lambda$. The size distribution is a function of particle size, and in general is a function of altitude, Z. The aerosol number concentration and the shape of the size distribution change with altitude. In MODTRAN the calculation of the normalised attenuation coefficients is done independently of the calculation of the vertical profile of the aerosol concentration. The aerosol attenuation coefficient is defined as the product of an altitude dependent aerosol concentration (scaling factor), $s(Z)$ (Fig. 1) and a wavelength dependent normalised aerosol attenuation coefficient $k_{atn}(\lambda)$

$$\beta_{atn}(Z,\lambda) = s(Z)k_{atn}(\lambda)$$

where $atn = ext$ or $abs$. The scaling factor is the extinction coefficient at 550 nanometres (nm). It is related to the surface meteorological range via the Koschmieder formula

$$VIS = \ln(1/\varepsilon)/(s(Z=0) + \beta_{ray})$$

where $\varepsilon = 0.02$ is the threshold contrast and in MODTRAN $\beta_{Ray} = 0.01159\ km^{-1}$ (in units of inverse kilometres, which is equal to $10^{-3}$ inverse metres) is the Rayleigh scattering coefficient for air at the surface for a wavelength of 550 nm. This is an approximation. The Rayleigh scattering coefficient for air will depend on the atmospheric conditions, in particular the absolute humidity. It is more accurate to use values for this quantity that are consistent with the model atmosphere used. This is done in MOSART for example. VIS is set for the default aerosol models. It can be overwritten in the MODTRAN input file. The scaling factor is a function of VIS, the season and the volcanic conditions.

The normalised attenuation coefficients are defined as ratios of the attenuation coefficients and the extinction coefficient at a wavelength of 550 nm:

$$k_{ext}(\lambda) = Ext(\lambda)/Ext(\lambda = 550nm) \text{ and } k_{abs}(\lambda) = Abs(\lambda)/Ext(\lambda = 550nm).$$

The extinction, absorption and asymmetry parameters shall be collectively referred to as the spectral parameters. To avoid confusion with other spectral quantities such as refractive index, they will be stated explicitly if necessary.

The spectral attenuation coefficients are computed at seven hundred and eighty eight wavelengths between 0.2 and 300 μm and for a range of RH (0, 70, 80 and 99%) and stored in MODTRAN for each of the aerosol models: rural, urban and maritime. The vertical aerosol profile (defined by $s(Z)$) is computed for different values of VIS: 2, 5, 10, 23 and 50 km. The upper altitude profiles are computed as a function of the season and volcanic conditions and stored in MODTRAN. Attenuation coefficients that are required at other values of RH and VIS are interpolated from the precomputed ones.

In older versions of MODTRAN (pre version 3.7) the user was able to include user defined aerosol profiles and or attenuation coefficients. If both quantities were being supplied then this had to be done in a self consistent way to ensure that the aerosol attenuation coefficient had the correct units of $km^{-1}$. For example the user could supply their own values for the aerosol scaling factor with AHAZE and their normalised attenuation coefficients with EXTC and ABSC. Only one user supplied aerosol profile could be included by using the user-selected profile option for the model atmosphere (MODEL=7). If the extinction, absorption and asymmetry parameters were being supplied by the user (IHAZE=7 option) then this could only be done for forty seven predefined wavelengths between 0.2 and 300 μm, limiting the spectral resolution.

In MODTRAN 3.7 the aerosol models can now be independently positioned to an arbitrary altitude region within the atmosphere. They can be stretched, compressed and scaled [3]. The advantage of this flexibility is that the inversion height and the tropopause can be more accurately modelled. This assumes the user knows the inversion height (if there is an inversion) and the height of the tropopause. This can be compared with MOSART for example, where the tropopause is accurately calculated in the model. The altitude regions have been decoupled from each other so independent aerosol profiles can be selected for each region and there can be overlap between profiles. This is referred to as the A+ option or upgrade

MODTRAN 3.7 includes the addition of a Stand-alone Mie code [19]. This allows the user to model the aerosol more realistically. Using the Mie code in conjunction with user supplied refractive indices as a function of wavelength or making use of the values given in the report by Shettle and Fenn, the user can now generate their own spectral parameters. The shape of the aerosol size distribution can be specified by the user. Current size distributions modelled include the modified gamma distribution, truncated power law and the sum of two and three log-normal distributions respectively.

The FORTRAN source code is located in the file mie2new.f. A sample input and out file is provided, along with data specifying the spectral index of refraction for a number of substances. These include the ones defined above for the aerosol models of Shettle and Fenn.

Further generalisations of the user-supplied spectral data include:

- the user can now supply spectral data on an arbitrary grid for the IHAZE=7 aerosol option

- the user can now supply spectral data for the default aerosol profiles as defined by IHAZE, ISEASN and IVUCLN (IHAZE ≠ 7 and ICLD ≠ 11) to avoid the need to rely on the sparse built-in databases of MODTRAN. This was possible in the past, but only at a fixed number of wavelengths (47). Now an arbitrary number of spectral parameters can be input to more accurately capture the spectral features present in some wavebands.

Both of these options are enabled by setting ARUSS = 'USS' in card 2 and are referred to as the USS upgrade. The other relevant cards are card 2D1 and card 2D2. The extinction and absorption coefficients in MODTRAN are dimensionless since they are divided by the extinction coefficient at 550 nm. This should be kept in mind when supplying externally generated attenuation coefficients.

The user can now input up to four user-defined aerosol profiles, lifting the previous restriction of one. This is done through the user-selected profile option for the model atmosphere (MODEL=7). It cannot be used with the A+ upgrade option which is only used to allow the user to shift around the built-in (default) aerosol models. As in the past these profiles can only be input as altitude-dependent aerosol extinction coefficients at 550 nm.

Finally the user supplied phase function input method has been upgraded. This upgrade is independent of the A+ and USS upgrades. The user supplied phase functions are now included as functions of both angle (as before) and wavelength.

# 3. Biomass Burning Aerosol (Smoke) Measurements from Jabiru

In 2003, DSTO in collaboration with the Commonwealth Scientific and Industrial Research Organisation (CSIRO) Division of Marine and Atmospheric Research, Queensland University of Technology and Airborne Research Australia conducted some aircraft measurements of the atmospheric aerosol around Jabiru [2]. Two measurement campaigns were conducted, one early during the dry season in June and the other towards the latter stages of the dry season in September.

Differences were observed in the aerosol characteristics between the two months. This was highlighted by the vertical profile of the aerosol number concentration and in the magnitude of the aerosol number concentration. The shape of the size distribution function also changed between the two months, signifying a different abundance of the contributing aerosol (fresh and aged smoke).

Limited aircraft flying hours, coupled with restrictions on the volumetric flow rate of the sampling equipment, and the isokinetic inlet, resulted in very low levels of aerosol mass being collected. This is also a result of the low level of aerosol mass suspended in the atmosphere around Jabiru. To compensate for these small quantities, flight leg samples were combined and in some cases multiple flights were combined. This increased the amount of mass

collected; sufficient to perform chemical analyses and to obtain reasonable counting statistics for the measured size distributions.

Three vertical regions were considered: the Lower Boundary (LB) layer, the Upper Boundary (UB) layer and the free troposphere (FT). The changes in the aerosol number concentration and in the shape of the size distribution were used to assist in assigning flight legs to each region. This was a dynamic process; the regions were not defined by fixed altitudes. Flight legs that were similar in nature were grouped together. Averages were then calculated over each region for the week in June and the week in September.

The details of the chemical analyses performed and the calculation of the campaign average size distributions can be found in the report by Carr et al. [2]. Here we just present the major results.

## 3.1 Chemical Composition of the Jabiru Aerosol

Analyses were performed to calculate the inorganic matter including soluble ions such as sodium ions and ammonium ions and elements such as potassium and calcium. Carbonaceous compounds were determined by a thermal-optical transmission (TOT) technique. The organic fraction, including the majority of the biomass smoke, was estimated by the level of the smoke tracer nssK (non sea salt potassium) as well as the missing mass from the Micro-Orifice Uniform Deposit Impactor (MOUDI) measurements [4].

The ground based size resolved chemistry data was used to derive size resolved particle density and refractive index. Additionally, it allowed for the identification of chemical species contributing to a particular size range. A chemical thermodynamic equilibrium model called SCAPE 2 [20] was used to determine the inorganic compounds present in the atmospheric aerosol under thermodynamic equilibrium. The results are presented as pie charts for each mode, region and month.

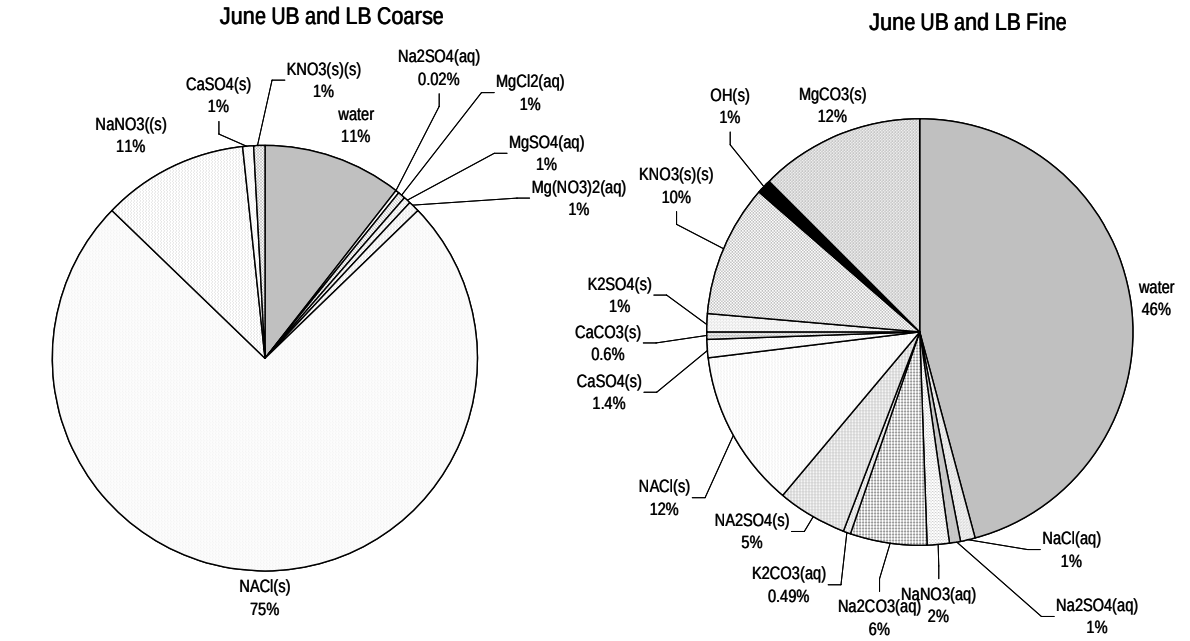


*Figure 2: The modelled compositions of the coarse and fine modes for the boundary layer for June. Water makes is a significant portion of the fine UB and LB aerosol. However, in the coarse UB and LB aerosol the composition is dominated by NaCl in the solid phase.*

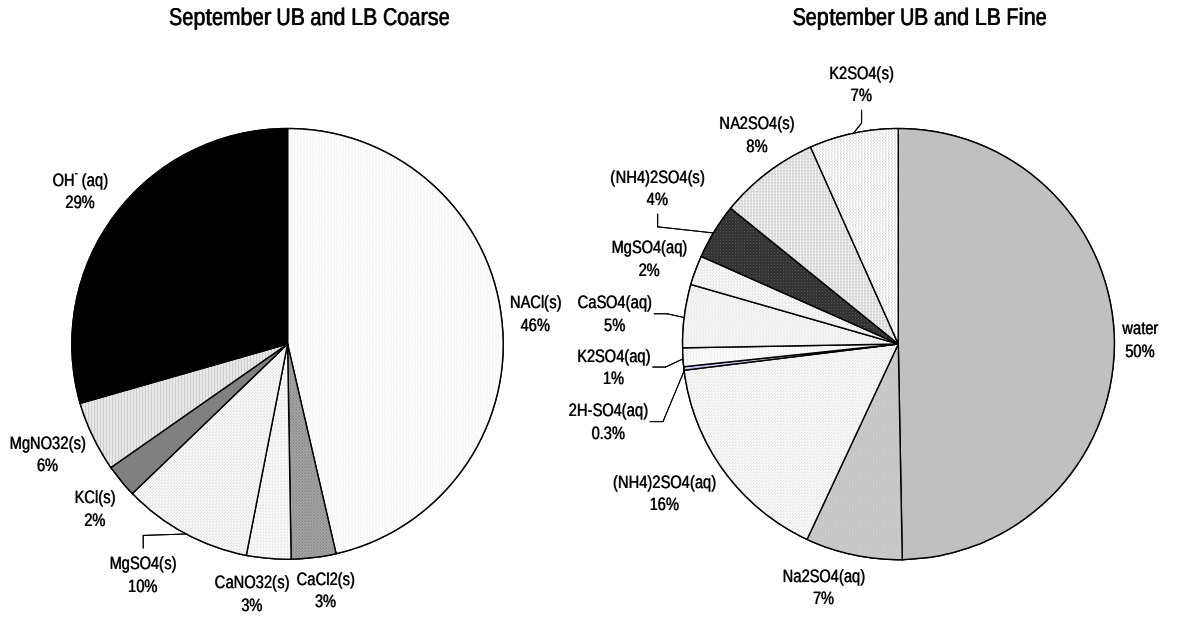


*Figure 3: Modelled compositions of the coarse and fine modes for the boundary for September. Water makes is a significant portion of the fine UB and LB aerosol.*

NaCl and carbonate species dominate the solid and aqueous phases of the June FT coarse aerosol. This is also the case for the June FT fine aerosol, with the addition of sodium sulphate species in both the solid and aqueous phases. The June UB and LB coarse aerosol modes are dominated by NaCl in the solid phase, with some $NaNO_3$ (representing the volatilization of Cl from sea salt during reaction with atmospheric $HNO_3$). The aqueous phase is minor, dominated by sulphate and nitrate species. The June UB and LB fine aerosol shows the solid phase dominated equally by NaCl, $MgCO_3$ and $KNO_3$. Less abundant sulphate species are again Na and K. The aqueous phase species are dominated by carbonates.

Aqueous species are absent from the September coarse and fine FT aerosol. For the coarse aerosol, NaCl and $NaHCO_3$ dominate, and the fine aerosol is exclusively made up of sulphate species. The aqueous phase of September coarse UB and LB aerosol is dominated by OH-, while most of the mass is dominated by NaCl and nitrate species in the solid phase. The fine September UB and LB aerosol is dominated by aqueous species, which are exclusively sulphate compounds.

The majority of the aerosol is composed of organic matter which is not included in the pie charts given above. The level of the smoke tracer nssK indicated that biomass smoke composed almost 100% of the fine mode aerosol.

The refractive index (at around 550 nm) and density were calculated using the results generated by SCAPE 2. The refractive index of a mixture can be determined by summing the partial molar refractivities for the individual compounds making up the mixture. Similarly, from the density of the individual species output by SCAPE 2, the density of the aerosol can be determined. The refractive index and density of the coarse and fine aerosol from the different atmospheric levels for the June and September campaigns are listed in Table 2.

*Table 2: Density and refractive index estimated for the coarse and fine particles from the different atmospheric levels for the June and September campaigns.*

| | density | Refractive Index | |
|---|---|---|---|
| | g $cm^{-3}$ | real | imaginary |
| | June | | |
| FT coarse | 1.54 | 1.542 | -0.00004 |
| FT fine | 1.43 | 1.548 | -0.00107 |
| UB and LB coarse | 1.50 | 1.549 | -0.00008 |
| UB and LB fine | 1.45 | 1.550 | -0.00236 |
| | September | | |
| FT coarse | 1.60 | 1.542 | -0.0005 |
| FT fine | 1.48 | 1.558 | -0.0106 |
| UB and LB coarse | 1.49 | 1.546 | -0.0003 |
| UB and LB fine | 1.46 | 1.552 | -0.0054 |

## 3.2 Particle Number Size Distributions

The measured size distributions were best represented by fitting lognormal distribution functions to the individual modes. No attempt was made to combine the distributions into one continuous function. For the coarse mode a Junge (power law) size distribution could equally have been chosen. The choice of a lognormal distribution for the coarse mode is consistent with the data.

The main observation is the presence of two modes corresponding most likely to a fresh smoke or Aitken mode and an aged smoke or accumulation mode. These two modes are quite distinct from each other but overlap and vary in magnitude between the months of June and September. Most notably in June the two modes are approximately the same in magnitude and hence as a result of an overlap in size range the resultant distribution appears like a flattened distribution (platykurtic). In September the accumulation mode dominates the smaller Aitken mode which forms a shoulder on the accumulation mode [2]. These results are presented in Figures 4 and 5.

The lognormal size distribution has the following functional form

$$\frac{dN(D;A_i,D_{m_i},\sigma_i)}{d\log D}=\frac{A_i}{\log(\xi_i)\sqrt{2\pi}}\exp\left[\frac{-(\log D-\log(D_{m_i}))^2}{2(\log(\xi_i))^2}\right]$$

with $A_i$ the total number of particles in the mode, the count median diameter (or geometric mean diameter) given by $D_{m_i}$ and the geometric standard deviation by $\xi_i$. The parameters of the size distributions are given in Tables 3 and 4.

*Table 3: The parameters of the fitted lognormal size distribution function for the fine mode aerosol. For the boundary layer regions in September two sets of data are presented corresponding to treating the Aitken and accumulation modes separately and treating the fine mode as one mode. A is $\#/cm^3$ and D is in $\mu m$.*

| *Distribution* | $A_1$ | $D_{m_1}$ | $\xi_1$ | $A_2$ | $D_{m_2}$ | $\xi_2$ | $A$ | $D_m$ | $\xi$ |
|---|---|---|---|---|---|---|---|---|---|
| June 03 | | | | | | | | | |
| LB | 630 | 0.078 | 1.785 | 575 | 0.112 | 1.669 | | | |
| UB | 345 | 0.060 | 1.940 | 173 | 0.110 | 1.534 | | | |
| FT | | | | | | | 397 | 0.059 | 1.743 |
| Sept 03 | | | | | | | | | |
| LB | 795 | 0.101 | 1.533 | 1170 | 0.131 | 1.591 | 1240 | 0.126 | 1.655 |
| UB | 355 | 0.085 | 1.687 | 522 | 0.138 | 1.546 | 652 | 0.122 | 1.892 |
| FT | | | | | | | 667 | 0.044 | 1.546 |

*Table 4: The parameters of the fitted lognormal volume and calculated size distribution functions for the coarse mode aerosol. $V_{A_c}$ is $\mu m^3/cm^3$, A is $\#/cm^3$ and D is in $\mu m$.*

| *Distribution* | $V_{A_c}$ | $D_{Vm_c}$ | $\xi_c$ | $A_c$ | $D_{m_c}$ |
|---|---|---|---|---|---|
| June 03 | | | | | |
| LB | 0.658 | 2.720 | 1.675 | 0.207 | 1.224 |
| UB | 0.141 | 2.658 | 1.680 | 0.048 | 1.184 |
| Sept 03 | | | | | |
| LB | 4.975 | 2.540 | 1.644 | 1.762 | 1.211 |
| UB | 1.033 | 2.535 | 1.610 | 0.336 | 1.283 |

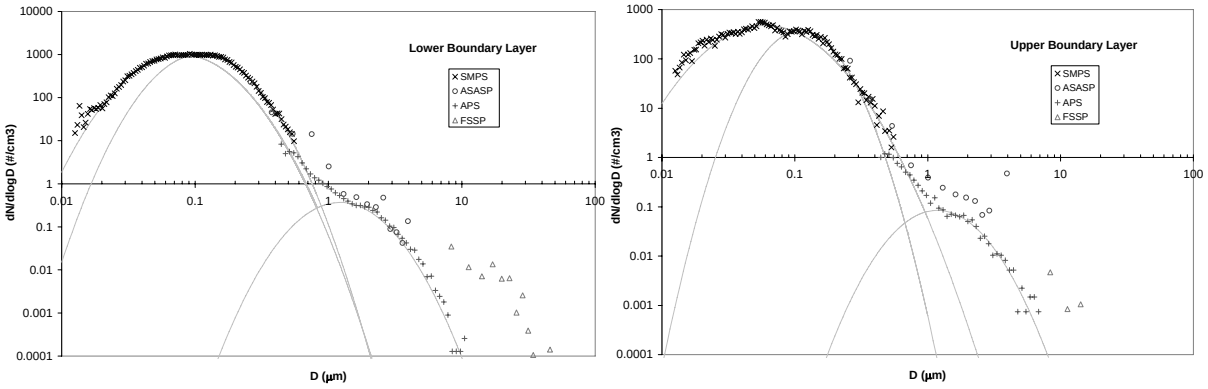


*Figure 4: Combined average size distributions for June 2003. Also displayed are the fitted lognormal functions for the various modes using the parameters from Tables 3 and 4.*

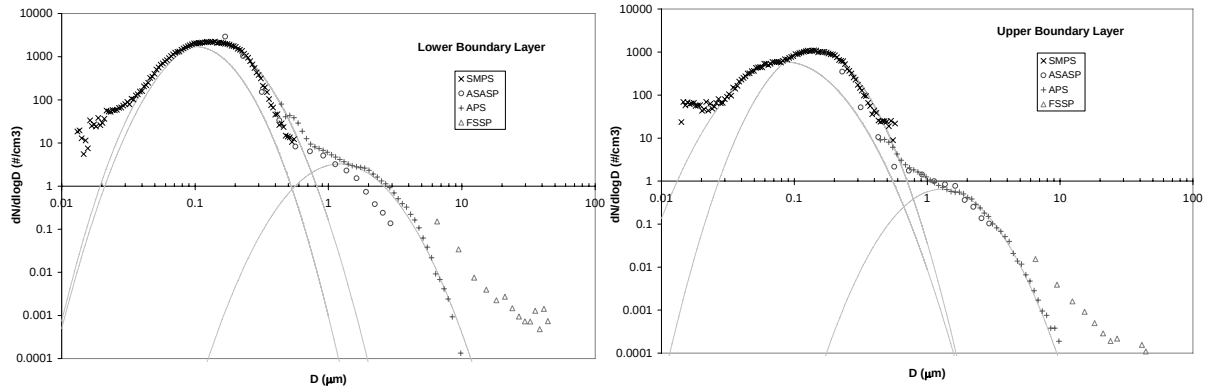


*Figure 5: Combined average size distributions for September 2003. Also displayed are the fitted lognormal functions for the various modes using the parameters from Tables 3 and 4.*

## 3.3 Biomass Burning Smoke Optical Properties

The type of biomass fuel sources around Jabiru are typically eucalyptus trees in open woodland configurations with an understorey of tussock type grasses [2]. The burning of these fuels is going to release amounts of organic and elemental carbon in the form of smoke. The term organic carbon is used to refer to carbon that is contained within organic molecules (containing carbon, hydrogen and oxygen in general). Elemental (or black) carbon, also referred to as soot, is pure carbon in the form of carbon chains for example. The purpose of the work done by Sutherland and Khanna [21] was to obtain measurements of the optical properties of organic-based aerosols produced by burning vegetation. They state in their paper that this is often overlooked in modelling the effects carbonaceous aerosol have on the atmospheric optical properties. In the case of biomass burning smoke one must consider the more complex organic carbon component of the aerosol along with the elemental carbon component. Summarising the results of Sutherland and Khanna they found that "regardless of the specific source type (of vegetation) all (transmission) spectra exhibited the same general features characteristic of complex organic compounds". The sources of vegetation they considered were alfalfa, mixed weed and lawn grass. They found that there were marked similarities and marked differences (in detail) between samples. Interestingly, they conclude that there is substantially less absorption in the far IR window indicating that the 10-12 μm region may be a better window through smoke than the 8-12 μm region. It is also worth mentioning that the two regions 2-2.5 and 4-5 μm are relatively void of strong absorption (for smoke). The spectral refractive index for both the alfalfa and mixed weed samples are given in their paper. They are considered representative of all the samples analysed. A listing of the mixed weed spectral refractive index from 2 to 17 μm at 25 $cm^{-1}$ intervals is also provided in their paper. These are listed in this report under organic carbon in Table 17 in Appendix A.

### 3.3.1 Smoke Refractive Index

The majority of smoke is composed of organic matter (containing organic carbon), elemental carbon (soot) and some water soluble compounds. We follow the procedure used in the paper by Trentmann et al. [22] to determine a composite biomass smoke refractive index. For black carbon the values from Shettle and Fenn's soot model are used. For wavelengths between 2 and 19 μm the values in the paper by Sutherland and Khanna [21] for organic carbon are used (Table 17, Appendix A). These values appear in the HITRAN (HIgh resolution TRANsmission) [23] database to account for non-volatile organic aerosols. Cubic spline interpolation is used to interpolate the real part of the refractive index to the values at the wavelengths used by Shettle and Fenn. For the imaginary part, linear interpolation is used, as this proved more accurate for longer wavelengths due to the nature of the variation of the imaginary part of the refractive index. For wavelengths between 1 and 2 μm and 19 and 40 μm the wavelength dependent refractive index of ammonium sulfate from Toon et al. [24] is used to represent the organic carbon, following the work of Grant et al. [25]. The refractive index of ammonium sulfate shows a similar behaviour to organic carbon over the visible wavelengths [24]. The calculations of atmospheric transmission presented in this report apply to the visible, 3-5 μm and 8-12 μm wavebands. Any inaccuracy in using ammonium sulfate over the wavelengths specified above, will not impact on these calculations.

We differ from Trentmann et al. in the treatment of the refractive index over the visible (UV and near IR (NIR)) wavelengths, 0.2 to 1 μm. Instead of using the combination of the data used by Trentmann et al. the value for the refractive index of organic carbon taken from the SCAPE 2 input is used. The difference is not large. Trentmann et al. use values between 1.52 and 1.54 (with a zero imaginary part). The value for the refractive index used in the SCAPE 2 model was 1.55 for organic carbon.

Trentmann et al. used the Maxwell-Garnett mixing rule [26, 27] to combine the black carbon and organic carbon refractive index. At 550 nanometres (nm) they find the refractive index is

$$n = 1.55 - 0.034\,i$$

which can be compared to the Jabiru lower boundary layer fine mode refractive index for September (Table 2)

$$n = 1.552 - 0.0054\,i\,.$$

The break down of the Jabiru aerosol components is presented in Table 5. These percentages are based on the mass measurements made on the ground at Jabiru using the MOUDI.

*Table 5: The break down of the Jabiru fine (smoke) and coarse mode aerosol into component aerosols.*

| Mode | Organic Carbon | Soot | Water Soluble | Mineral Dust (soil) | Sea Salt |
|---|---|---|---|---|---|
| Fine | 70% | 20 % | <5 % | <5% | <5% |
| Coarse | <5% | <5% | 10% | 25-40 % | 25-40% |

The value of the composite refractive index obtained using the soot refractive index of Shettle and Fenn and calculating the volume weighted average refractive index assuming only soot and organic carbon is

$$n = 1.59 - 0.088\,i\,.$$

The imaginary component is relatively high, indicating an overestimation of elemental carbon. Assuming only 10% soot then the value for the complex refractive index is halved and

$$n = 1.57 - 0.044\,i\,.$$

Using a value of 1% for elemental carbon the composite refractive index at 550nm becomes

$$n = 1.552 - 0.0044\,i$$

in much better agreement with the calculated value from the Jabiru data (Table 2).

With the addition of small amounts of water soluble, mineral dust and sea salt components (5% each) and marginally reducing the organic component, the refractive index for the Jabiru smoke aerosol in the fine mode is

$$n = 1.548 - 0.0051i$$

which is close to the value obtained from measurements and SCAPE 2. The imaginary part is controlled primarily by the soot component. The real part varies between 1.55 and 1.6 while the imaginary part changes by an order of magnitude depending on the percentage of soot. Two values of smoke spectral refractive index are chosen corresponding to smoke that has a high soot component (10%) versus smoke that has a relatively low soot component (1%). Due to the fact the imaginary part is small this may have little impact on the calculated attenuation coefficients and atmospheric transmission calculations. The smoke spectral refractive index is shown along with the coarse mode refractive index in Figure 6.

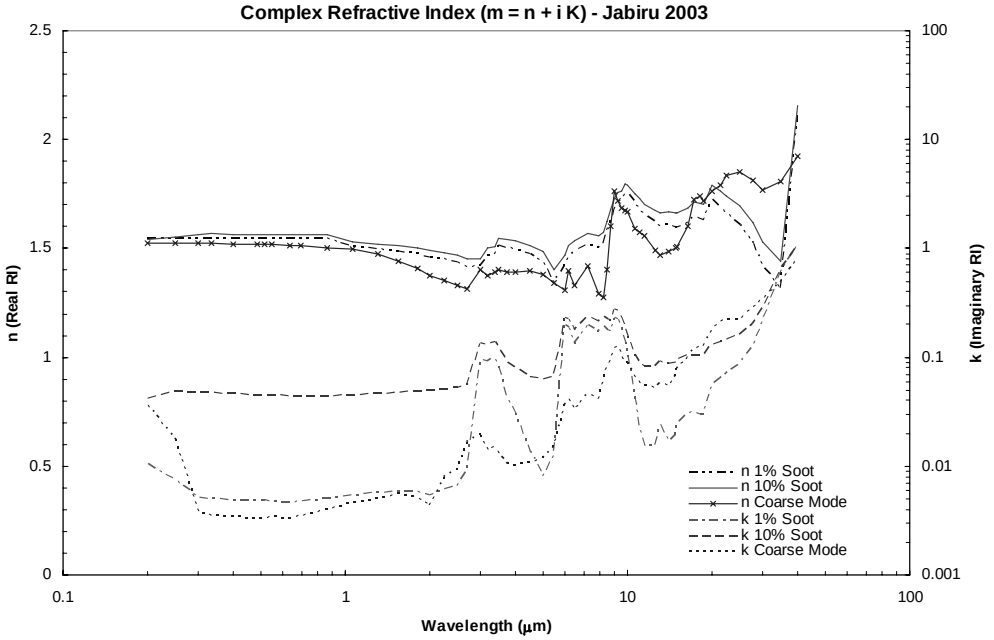


*Figure 6: The real and imaginary components of the Jabiru spectral refractive indices for the 1% soot smoke, the 10% soot smoke and the coarse mode.*

The refractive indices have been calculated as volume weighted averages of the component refractive indices given in Table 5 for the fine mode. There are numerous techniques for combining component refractive indices to get the refractive index of a composite aerosol. These include calculating the volume weighted average (as we have done) and the Maxwell-Garnet mixing rule [27, 28, 29]. Much literature has been devoted to the determination of the aerosol mixture refractive index assuming combinations of external, internal, uniform and inhomogeneous mixtures [30, 31, 32]. The details of these methods are beyond the scope of

this report. We mention them here to highlight that the method we chose to determine a composite aerosol refractive index is not the only one.

Maenhaut et al. [33] performed an absolute principal component analysis (APCA) and chemical mass balance (CMB) receptor model study to identify the major aerosol components (source types) for both fine and coarse mode fractions in Jabiru. This analysis was based on measurements with a Gent PM10 SFU (particulate mass for diameters less than 10 μm stacked filter unit) over an 18 month period from mid-may 1995 until December 1996. Samples were typically collected over 3 days. The coarse and fine filters were analysed for particulate mass, black carbon and over 40 elements. Similar components were identified to those measured at Jabiru during 2003.

*Table 6: Aerosol sources at Jabiru (1995-1996).*

| *Component %* | *Fine particle fraction (83% accounted for)* | *Coarse Particle fraction (67% accounted for)* |
|---|---|---|
| Biomass burning (dry season) | 60% | |
| Sulphate | | 4% |
| Mineral Dust | | 36% |
| Sea Salt | | 27% |

The four components listed above explain on average 83% of the fine particulate mass. Part of this missing mass is likely to be attributable to biogenic organic aerosol and to nitrates.

The results obtained during 2003 show a higher smoke level than these measurements. This is probably due to the fact that the 2003 measurements were undertaken in the dry season when biomass burning is ubiquitous. The results of Maenhaut et al. are averages over both dry and wet seasons. The coarse mode agreement is quite good, although there is large uncertainty in our weighted percentages. This is unlikely to have a significant impact on optical calculations, due to the very small coarse mode number concentration.

# 4. Calculating the Spectral Attenuation Coefficients for the Jabiru (Smoke) Aerosol

The calculation of the spectral attenuation coefficients in MODTRAN requires two quantities:

1. the particle number size distribution
2. the extinction and absorption cross sections for a single particle.

The cross section is a function of particle diameter and wavelength. The scattering coefficient of the aerosol was measured at three visible wavelengths 450, 550 and 700 nm. The absorption coefficient was measured at 530 nm. To make full use of the aerosol models in MODTRAN a determination of the spectral attenuation coefficients over all wavelengths of interest is necessary. The measurements of the scattering and absorption coefficients are not general

enough for this purpose. Combining the measurements of the size distribution and the determination of the chemical composition of the aerosol with a theoretical model enables a calculation of the cross section as a function of wavelength. The procedure followed here is used in MODTRAN. Mie scattering theory is used to calculate the cross sections for extinction and scattering as functions of particle size and wavelength. These are then combined with theoretical size distribution functions; the parameters of which have been determined in fits to measurements of the size distribution. In this report only the lower boundary layer region size distribution measurements are considered.

## 4.1 Mie Scattering Theory

The classical theory describing the scattering of electromagnetic radiation by a sphere was developed in the early part of the 20th century by Gustav Mie [17]. Ludwig Lorenz independently developed the theory of scattering of plane electromagnetic waves by metallic spheres. We adopt the standard convention of referring to the scattering of light by spheres as Mie scattering theory. Often it is referred to as the Lorenz-Mie theory. Quantum mechanics is the correct theory to use to describe the interaction of light (photons) with matter (atoms, molecules and solids). Results of classical physics produce answers that agree with quantum physics under many circumstances. The scattering of light by a sphere is one such example. For the purpose of deriving scattering and extinction cross sections for spheres of an arbitrary diameter, classical Mie scattering theory suffices and so we use it here.

The spectral refractive index determines the scattering properties of the sphere. The refractive index is dependent on the material the sphere is composed of. The aerosol particles in Jabiru contain inorganic and organic compounds and elemental carbon from biomass burning. In general the refractive index is complex, with the imaginary part representing attenuation of the wave inside the sphere, accounting for absorption of some of the incident EM energy.

To represent the aerosol particles as spheres is a simplifying assumption. Many aerosol particles are not spherical, such as square shaped salt crystals. The effects of particle shape irregularities tend to be averaged out in calculations in the atmosphere if the particles are well suspended in a turbulent media (such as the atmosphere under certain conditions). In this case they are being continually mixed and are not orientated in a particular direction. Mie theory is employed by utilising the stand alone Mie code provided with the MODTRAN distribution. The basic results of Mie theory are presented without derivation. For more information the reader is referred to the many standard texts on the subject, such as the book by Bohren and Huffman [18].

The attenuation coefficients are functions of the cross sections for extinction and absorption and the physical size distribution. Mie theory enables the calculation of the scattering cross section and the extinction cross section. The absorption cross section is obtained as the difference between the extinction and scattering cross sections. Dividing these cross sections by the geometric cross section for a sphere ($\pi r^2$), the scattering and extinction efficiency factors are obtained:

$$Q_{atn}\left(m(\lambda), x\right) = \sigma_{atn}\left(m(\lambda), x\right) / \pi r^2 ;\ atn = ext\ or\ scat$$

where $Q_{atn}$ is the efficiency and $\sigma_{atn}$ is the cross section for attenuation respectively. Both quantities are functions of complex spectral refractive index, $m(\lambda) = n(\lambda) + i\,k(\lambda)$ and particle size through the Mie size parameter, $x = 2\pi r / \lambda$.

The explicit form for the efficiency factors is as follows

$$Q_{scat} = \frac{2}{x^2}\sum_{n=1}^{\infty}(2n+1)\left(|a_n|^2 + |b_n|^2\right)$$

$$Q_{ext} = \frac{2}{x^2}\sum_{n=1}^{\infty}(2n+1)\mathrm{Re}\{a_n + b_n\}.$$

The functions $a_n$ and $b_n$ are given in terms of the complex index of refraction and the Ricatti-Bessel functions. The Ricatti-Bessel functions are dependent on the Mie size parameter $x$. Recursion relationships can be derived for $a_n$ and $b_n$. This aids in the numerical computation of the efficiencies. These series can be slowly converging. Careful treatment of the numerical analysis is needed to ensure that stable and convergent solutions are obtained. The stand alone Mie code mie2new.f is able to account for a wide range of scenarios.

The attenuation coefficients are obtained by integration of the attenuation cross section over the size distribution as follows:

$$\beta_{atn}(\lambda) = \int_0^{\infty} dr\ \sigma_{atn}(m(\lambda), r)\, n(r)$$

$$\equiv \int_0^{\infty} dr\ \pi r^2\ Q_{atn}(m(\lambda), r)\, n(r)$$

where $atn = ext\ or\ scat$ and $n(r) = \dfrac{dN(r)}{dr}$ is the differential number size distribution.

## 4.2 Spectral Refractive Indices

An extensive literature survey of measurements of refractive indices of a range of compounds including elemental carbon (soot), water soluble species, sea salt and dust was undertaken by Shettle and Fenn. These are catalogued in their report [14].

The dust component aerosol refractive index used by Shettle and Fenn is taken from the measurements of Volz [34, 35]. No information is given as to the exact dust measurements of Volz that are used. The HITRAN database is accompanied by a table of spectral refractive indices for the component aerosol models of Shettle and Fenn. The references that accompany the HITRAN data base for the dust like aerosol refractive index refer to the report of Shettle and Fenn and to a third reference of Volz [36]. The conclusion is that the dust like aerosol refractive index could be that obtained from rain and snow water sedimentation measurements or Saharan dust samples collected at Barbados in the Caribbean, following long

range transport. A third source seems to indicate that it is the Saharan dust measurements that are used to determine the dust-like refractive index [37].

In d'Almeida et al. [37] a separate mineral aerosol refractive index more representative of crustal derived mineral is used. This model is based on the measurements of Grams et al. [38] and Patterson et al. [39] over the UV and visible wavelengths. The measurements of Volz are used over the IR wavelengths and beyond. This is justified on the basis that the measurements of the dust-like refractive index correspond to soil derived aerosol. In d'Almeida et al. it is explicitly stated that the dust-like (referring to the dust like model of Shettle and Fenn) substances are mineral dust found in non-desert locations representing mid latitude soil conditions. The mineral and dust-like models only differ over the visible wavelengths. In Highwood et al. [40], the refractive index of the WCP-112 [40] dust like aerosol (identical to the one in Shettle and Fenn) differs from the refractive index obtained from the measurements of Volz for a Saharan dust collected at Barbados over the 7-16.5 μm range. The implication is that the dust-like model of Shettle and Fenn is not composed solely of the Saharan dust measurements of Volz but must include some of the other dust measurements of Volz.

The dust-like model of Shettle and Fenn is chosen to represent our mineral dust aerosol refractive index. This is consistent with the literature. Haywood et al. [42] claim that the imaginary component of the dust-like refractive index is significantly overestimated in the WCP-112 dust-like aerosol model. Based on measurements, they have adjusted the imaginary component of the refractive index from 0.008 to 0.0015 in the wavelength range 0.3-2 μm. We use the adjustment made by Haywood et al. because it fits our measurements better. This is referred to as the modified dust-like aerosol. It is in better agreement with the mineral aerosol refractive index of d'Almeida et al. over that wavelength range.

Additional measurements of mineral dust exist, such as those reported by Myhre et al [43]. Values for the refractive index over visible wavelengths are taken from the retrieval of aerosol column averaged size distributions and from sun photometer measurements. The refractive index of Fouquart et al. [44] is used over thermal wavelengths. The latter appear in Highwood et al. The refractive index of Fouquart et al. includes measurements from other sources, including Volz, over the 8-14 μm range. Prima facie this contradicts the data given in Highwood et al., where a difference is observed between the refractive index of Volz and Fouquart over the 7 to 16.5 μm range.

Table 5 contains the percentage amounts (by volume) of the basic components of the Jabiru aerosol. The coarse mode is predominantly sea-salt and mineral dust and the fine mode predominantly biomass smoke composed of organic carbon plus a small soot component.

The aerosol mass density and refractive index for the LB region are similar for June and September (Table 2). The imaginary part of the fine mode refractive index for September is about double the value reported for June. The magnitude is small, 0.0054, and should have little impact on atmospheric transmission calculations. For the calculations in this report we chose a single composite aerosol particle for June and September. The seasonal changes in the aerosol properties will manifest themselves in the size distributions used for each month.

The uncertainty in the percentage components comprising the coarse mode reflects the difficulty in determining composition based on such small amounts of measured mass. To reproduce a value for the coarse mode refractive Index close to the measured value at 550 nm we have adjusted the percentages slightly.

The smoke aerosol refractive index (for 1% and 10% soot) is used as the Jabiru fine mode aerosol. The coarse mode aerosol particle is assumed to be composed of 45% sea salt, 40% mineral dust, 10% water soluble material, 5% organic carbon and a small amount of elemental carbon (0.5%) (Fig. 6). These values are consistent with the values given in Table 5. The coarse mode refractive index is then calculated as a volume weighted average of these component refractive indices.

The coarse mode composite aerosol particle has an imaginary refractive index component that is an order of magnitude larger than the measured refractive index. The component that is the least well understood is the water soluble aerosol. There is no other data available on the spectral refractive index for water soluble aerosol (that we are aware of). If such data becomes available, the calculation of the coarse mode refractive index should be redone.

## 4.3 The Multimode Size Distributions

Three modes were identified: the Aitken, accumulation and coarse modes. Lognormal size distribution functions were fitted to each mode separately. These results are presented in Chapter 3. The true size distribution function is a sum of three lognormal size distribution functions. This results in a total of nine parameters that need to be determined. A MATLAB® (© 1994-2005 The MathWorks, Inc.) program was written to fit each mode individually. It is not suitable to be used to determine a fit of the sum of three lognormals. The software package DistFit (Chimera Technologies, Inc. © 1988-2004) is used for this purpose. DistFit is used to manipulate size distribution data and to fit such data to one or more superimposed size distribution functions using a simplex fitting algorithm [45]. It was used in the manual fitting mode, forcing a fit to the sum of three lognormal size distributions. To help constrain the fit, the geometric mean diameters of the three modes were fixed at the values obtained from the fits to the individual modes. DistFit is able to reproduce the fits to the individual modes. This required truncating the upper and lower diameters.

To determine the six remaining parameters, a simultaneous fit to the data is made using DistFit. The distribution function has the form

$$\frac{dN(D)}{d\log D} = \sum_{i=1}^{3} \frac{N_i}{\log(\xi_i)\sqrt{2\pi}} \exp\left[\frac{-(\log D - \log(D_{m_i}))^2}{2(\log(\xi_i))^2}\right]$$

The parameters that define this distribution function are given in Table 7.

Two fits were made to the data. In the first case (Fit 1) the data was not truncated. In the second case (Fit 2) the data was truncated below 0.03 μm and above 4.5 μm. Data between 0.4 and 1.5 μm was excluded. The reason this data was excluded is because it is likely to be

inaccurate. The difference between the two fits is not significant for September; except at the extremes of the size distribution. In June the APS data was the noisiest and the difference is quite marked. Fit 2 is used in further calculations.

*Table 7: The parameters of the fitted size distribution function for the Jabiru aerosol. In this case the sum of three lognormals for the Aitken, accumulation and coarse modes. N is $\#/cm^3$ and D is in μm.*

| *Distribution* | $N_1$ | $D_{m_1}$ | $\xi_1$ | $N_2$ | $D_{m_2}$ | $\xi_2$ | $N_3$ | $D_{m_3}$ | $\xi_3$ |
|---|---|---|---|---|---|---|---|---|---|
| June 03 - LB | | | | | | | | | |
| Fit 1 | 484 | 0.078 | 1.91 | 270 | 0.112 | 1.70 | 0.112 | 1.22 | 1.31 |
| Fit 2 | 535 | 0.078 | 2.02 | 235 | 0.112 | 1.66 | 0.186 | 1.22 | 1.69 |
| Sept 03 - LB | | | | | | | | | |
| Fit 1 | 374 | 0.101 | 1.79 | 849 | 0.131 | 1.52 | 2.01 | 1.21 | 1.55 |
| Fit 2 | 340 | 0.101 | 1.74 | 884 | 0.131 | 1.55 | 1.75 | 1.21 | 1.61 |

The agreement with the measurements is quite good (Fig. 7). The data from the SMPS and the APS is displayed; this data was used to constrain the fits. Fit 2 produces the better agreement with the data for June. The major discrepancy between the fitted functions and the data is where the accumulation mode and coarse mode overlap around 0.5 to 1 μm. This is due to the need to truncate the data for the APS due to counting inefficiencies with the instrument and hence the fit is poorly constrained over this region. This is particularly the case for September. Fit 1 is no better, highlighting how difficult it is to produce a fit of the sum of three log normal size distribution functions to the data.

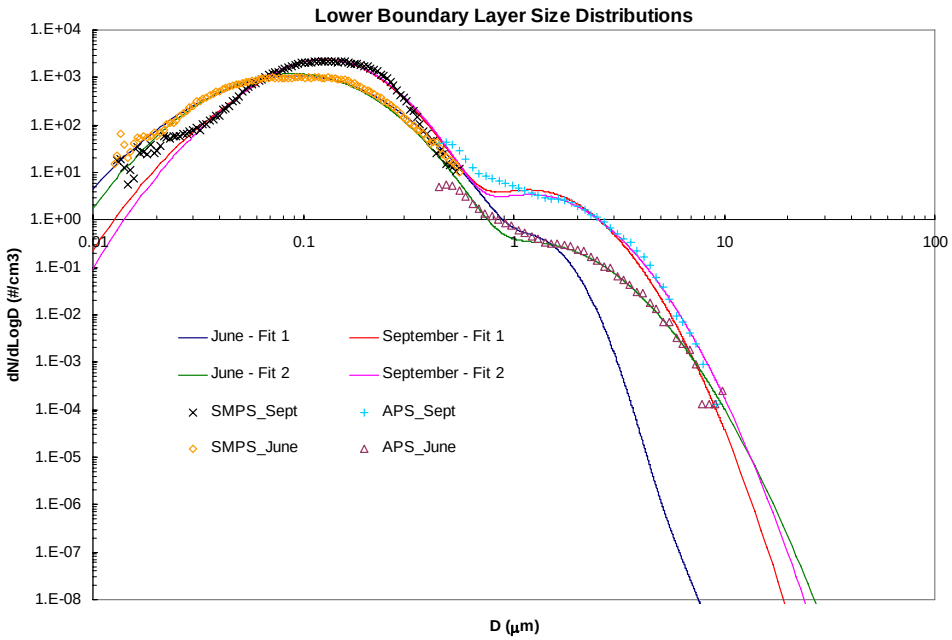


*Figure 7: The fitted size distribution functions for the lower boundary layer for both June and September 2003 and size distribution data from the SMPS and the APS.*

### 4.3.1 Comments on the Size Distributions

The instruments that measure the size distribution have limitations. In particular, the Scanning Mobility Particle Sizer (SMPS) has a lower size limit cut off, which is a function of ambient pressure, increasing for higher altitudes [2]. The lower size cut off may mask the existence of a real nucleation mode. All measurements of the total number of particles will be sensitive to this lower limit, since the fine mode tends to dominate the number concentration. The size distribution data has a sharp drop below around 0.01 μm. This may be due to the absence of a nucleation mode or to the lower size cut-off of the SMPS. The effect of these size particles (<0.01) on the scattering of light is small, in general.

The Jabiru aerosol calculations are based on a specific set of measurements. Therefore they do not represent a true model in the sense of the models of Shettle and Fenn, which are more general in their construction. The aerosol models in MODTRAN are not derived from one set of measurements. The lower size limit will therefore depend upon any assumptions made as to the assumed distribution of the smallest particles.

The total number concentration for the Jabiru fine mode measurements (Table 8) is substantially smaller than for a typical boundary layer aerosol model of Shettle and Fenn. This relatively small particle number concentration translates to a VIS of over 100 km in the boundary layer. These conclusions are based on the campaign average number distributions and boundary layer (lower boundary layer region) scattering coefficients (from the nephelometer). The VIS closer to the vicinity of smoke plumes will be lower.

*Table 8: Average Number concentration of Jabiru aerosol in the boundary layer low region. Note these are from the measurements, not the fitted size distribution functions.*

| Campaign | Number Concentration $cm^{-3}$ | |
|---|---|---|
| | Fine Mode (SMPS) | Coarse Mode (APS) |
| | | |
| June | 793.44 | 3.24 |
| | | |
| September | 1241.71 | 21.71 |

The RH was relatively low inside the instruments. Both the SMPS and the aerodynamic particle sizer (APS) [2] sample heated air due to aspiration at the isokinetic inlet entrance and due to the transport of the sample air through the conductive silicon tube. There is some heating due to the instruments. Neither of these instruments records sample RH. The nephelometer does record sample RH. The nephelometer RH should be a reasonable approximation to the RH inside the other instruments. These values ranged between 39 and 67% for the lower boundary layer flights in September and between 16 and 28% in June. The averages were around 50% and 22% respectively. The difference between a dry aerosol scattering coefficient and an aerosol scattering coefficient at 50% RH is not large. This corresponds to a region of the RH growth (f(RH)) curve that is essentially flat .

### 4.3.2 Smoky Region Size Distribution

The size distributions have been obtained using averages over multiple flight legs and flights for each campaign. This represents average smoke aerosol size distributions for the region. They do not represent the size distribution in a smoky region (that is near a fire or fire front). The averages will contain large plume samples; these will be averaged out by the background samples. This is particularly the case for June since the background smoke concentration in the haze layer was lower than for September. To take account of the effect imaging through a smoky region may have on performance a smoky region size distribution has been modelled.

The chemical composition of the aerosol in the smoky region is assumed to be the same as elsewhere in the haze layer. The only difference is likely to be a higher number concentration and perhaps a difference in the shape of the size distribution compared with the average size distributions.

The only suitable measurements, that could be considered to be from a region obviously dominated by a series of fires, were obtained in June. We have chosen to calculate an average size distribution obtained from a single leg that was flown in a region that was dominated by fires. This flight leg was chosen specifically because it was observed on that day there was a greater prevalence of fires over this region than the region around Jabiru. This option is preferred over taking a single plume sample. It represents a very smoky region of the boundary layer over an extended path giving a better representation of the aerosol size distribution under such conditions. Furthermore by averaging over a number of samples the possibility of a single sample anomaly is avoided.

DistFit is used to obtain a fit to the sum of three lognormals. The size distribution in the fine mode has a sharp peak (leptokurtic) and it is not clear where the two modes (if in fact there are two modes) geometric mean diameters are located (it is hard to separate the modes by inspection). To fit the fine mode it was advantageous to use the auto fit option in DistFit up to a maximum of two lognormals. The procedure does not produce a good fit to the data. The coarse mode fit was done independently by truncating the data below about 1.5 μm and above 4.5 μm as has been done consistently in the past. DistFit was able to return a single mode fit to the coarse mode. As DistFit could not produce a bimodal fit to the fine mode when treated separately from the coarse mode it was decided to fit all the data simultaneously using the auto fit option in DisFit (up to a maximum of three lognormals).

*Table 9: The parameters of the smoky region size distribution function.*

| Distribution | $N_1$ | $D_{m_1}$ | $\xi_1$ | $N_2$ | $D_{m_2}$ | $\xi_2$ | $N_3$ | $D_{m_3}$ | $\xi_3$ |
|---|---|---|---|---|---|---|---|---|---|
| Smoky Region | 1938 | 0.094 | 1.75 | 523 | 0.117 | 1.22 | 0.223 | 1.51 | 1.45 |

This method produced a better fit to the fine mode, and the coarse mode parameters were very similar to the individual coarse mode fit. The results are sensitive to the required $\chi^2$; if it is set too high then only one mode is used to fit the entire set of size distribution data. Therefore an understanding of the physics behind the modes of the size distribution is

necessary to ensure that DistFit produces something that mathematically and physically makes sense. The data does not show a single lognormal distribution (not a rounded peak but a rather sharp top) which indicates more than one mode is present. This could also be an artefact of the SMPS sampling since the instrument takes 120 seconds to complete an electronic scan of the size range. The aircraft can move about 6 km in 1 minute as a result of which higher smoke concentrations may have been measured for some parts of the size distribution than others, due to the fact the SMPS is translated a large distance during the measurement of one single sample. This artefact will have been averaged out for the June and September average size distributions but not necessarily over the single flight leg.

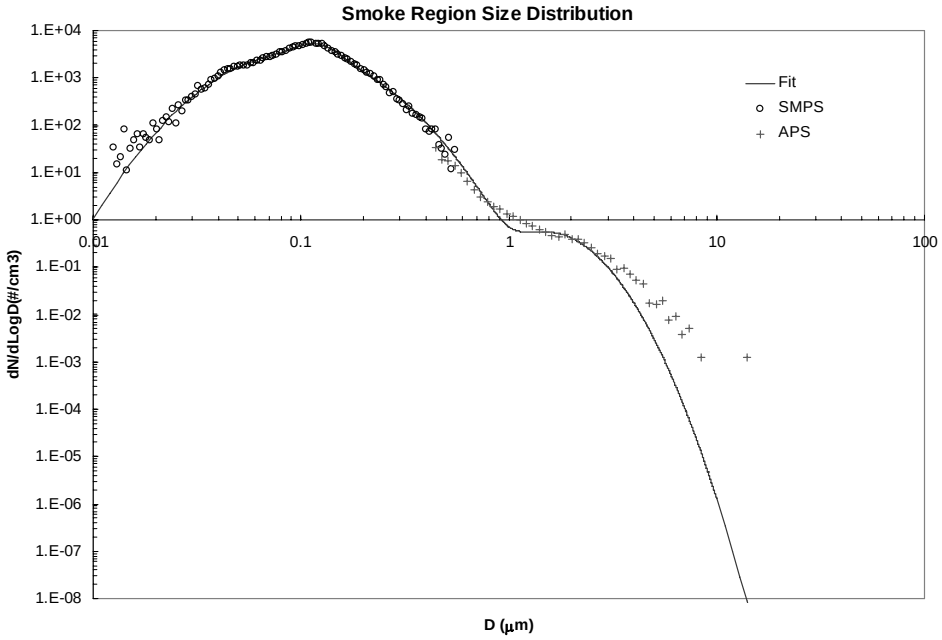


*Figure 8: The fitted smoky region size distribution function and size distribution data from the SMPS and the APS.*

## 4.4 The Attenuation Coefficients

The stand alone Mie scattering code called mie2new.f is used to calculate aerosol extinction, scattering and absorption coefficients and asymmetry parameters. This code is provided with MODTRAN in a separate directory called mie. It is based on a program developed by RRA Fort Worth, Texas. It has been revised a number of times first by E. Shettle et al. of the AFGL and then by M. W. Mathew of Spectral Sciences, Inc. The code is well commented and it is straightforward to use. The code was compiled and executed on a SunOS 5.9 Unix platform using the GNU f77 (Fortran 77) compiler. The f90 (Fortran 90) compiler when operated in f77 mode had problems linking the object files. The problem with the f90 compiler can be overcome by obtaining a suitable patch. The input file to this program is referred to as mie2new.tp5 (analogous to the tape 5 input file in MODTRAN itself) and the output files are called mie2new.tp6 (tp6) and mie2new.tp8 (tp8) respectively. The output file tp6 contains

more verbose information than is provided in the tp8 file. The input file tp5 contains a number of lines. Each line corresponds to a card. The details of what each card does are given in the report [16] that accompanies the Mie code. This is located in the mie directory. An example mie2new.tp5 file is provided in Appendix B. As with MODTRAN, it is tedious and frustrating when formatting the various cards correctly. The output files do not provide the attenuation coefficients in a convenient form to be immediately imported into Excel, for example, and plotted. The majority of the effort in running the Mie code is involved in these two processes.

The attenuation coefficients are evaluated at sixty one spectral grid points (wavelengths) corresponding to the values of the spectral refractive index. The spectral refractive index of smoke and the fitted size distributions (for June and September) are taken as input. No further consideration is given to the smoky region aerosol model. This is because the VIS predicted by this model is larger than the 1% soot smoke model for September. Nothing is to be gained in performing calculations using the smoky region aerosol model. The sum of three log normals option is selected by setting NEQ = 4. The parameters in Table 7 are taken as input in the tp5 file. First a conversion of the geometric mean diameters to geometric mean radii was made. Before attempting a calculation of the attenuation coefficients at all wavelengths, a partial optimization of the parameters in the Mie code was undertaken. This was done for the 1% soot smoke aerosol for September at 550 nm. The parameters adjusted were the minimum and maximum radii to be integrated over (rmin and rmax), the number of steps to be used when integrating over the aerosol size distribution and the number of angles used in calculating the angular integral over the phase function. Because computational performance is not a problem on a modern Sun platform, angular steps of $1^\circ$ between $0^\circ$ and $8^\circ$ and $2^\circ$ everywhere else are chosen. The maximum number of angles allowed is 150. The answers are not stable below around 129 radius steps. When using a large upper limit for rmax, convergence problems are reported in the Kronrod quadrature but the coefficients are still calculated. There is agreement to 2 significant figures between using rmin=0.001 and rmax=100, and rmin=0.01 and rmax=50. The choice of rmin=0.001 and rmax=50 was made. In all cases, underflow errors are reported when running the executable mie2new.exe.

The theoretical size distribution functions are continuous and differentiable (smooth) functions of particle radius. The Mie attenuation efficiency factors can demonstrate variable behaviour as a function of the Mie size parameter ( $x = 2\pi r / \lambda$ ). This may prevent a stable integral calculation. Wiscombe refers to spikes in the efficiency factors corresponding to a resonance [46]. It is unknown how mie2new.f will cope with the situation where a radius step inadvertently hits a resonance present in the efficiency factor. As Kronrod quadrature are used (which are based on Gauss type quadrature) we can assume that for stable results the integrand needs to be a smooth function of radius. Therefore the user needs to pay careful attention to the numerical inputs and outputs of the code. It has been shown for our test case that the results are stable with changes in Nstep (above 129).

In this report the internally mixed aerosol model is used. To simplify the calculation the smoke aerosol composite refractive index is used over the entire size range. Alternatively the Mie calculation can be undertaken twice; using the portion of the size distribution corresponding to the fine mode and the smoke refractive index and then using the portion of the size distribution corresponding to the coarse mode and the Jabiru coarse mode refractive

index. The output of the two runs could then be combined using the linearity of the integral operator to get a total attenuation coefficient.

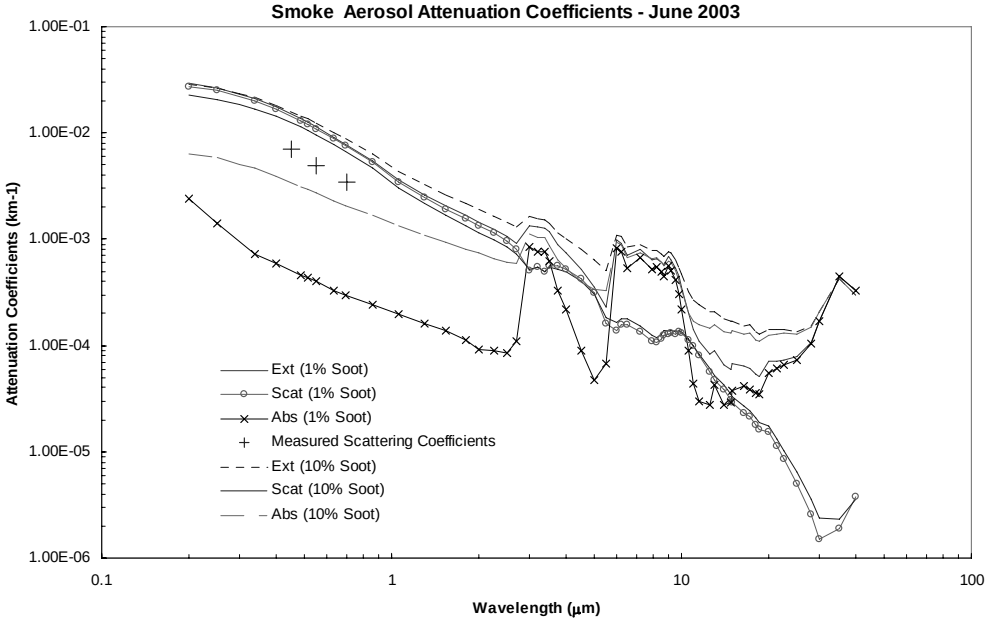


*Figure 9: The aerosol attenuation coefficients for the 1% and 10% soot smoke aerosols for June 2003. Also shown are the measurements obtained with the integrating nephelometer.*

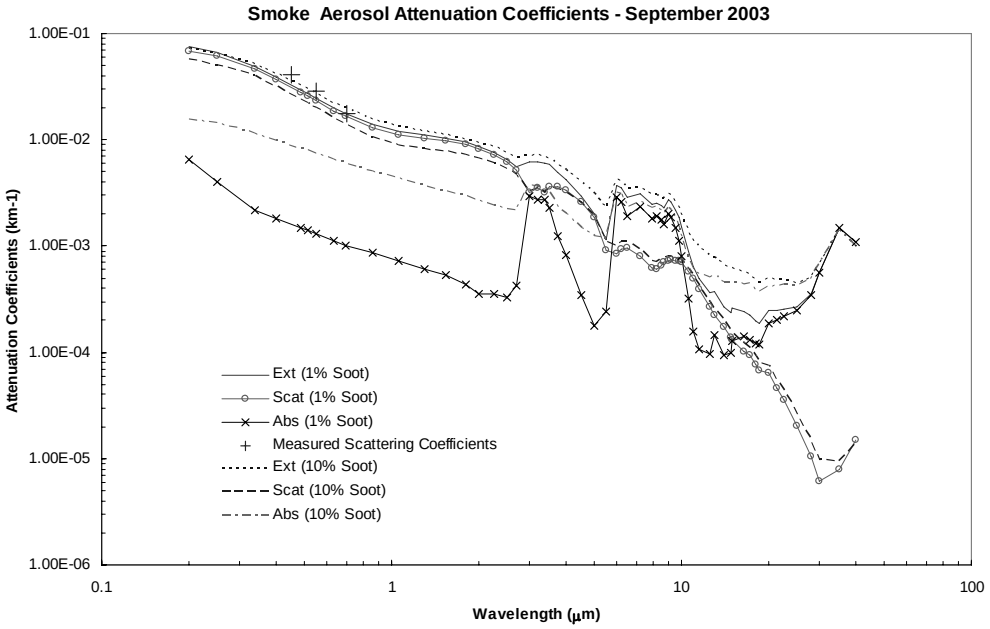


*Figure 10: The aerosol attenuation coefficients for the 1% and 10% soot smoke aerosols for September 2003. Also shown are the measurements obtained with the integrating nephelometer.*

Included in these figures are the measured values of the scattering coefficients at 450, 550 and 700 nm obtained using the three wavelength integrating nephelometer. The agreement is quite good for September. There is reasonable agreement for June. The magnitude of the scattering coefficients is different and the measured values are off-set from the calculated ones. In June regular background measurements (called zero baseline measurements (ZBM)) were not undertaken. As a result the instrument values of the wall scattering were not accurately known. This affects the measured scattering coefficients due to the fact that any effects due to contamination of the scattering chamber were not being accounted for. This could result in a fixed off-set; the ZBM are subtracted from the measured scattering coefficient (as well as the Rayleigh scattering coefficients) to obtain the scattering coefficient for aerosols.

The measured values have not been corrected for angular truncation error inside the nephelometer. RH effects have not been considered. Both are likely to result in increases in the values of the measured scattering coefficients. The RH effect may not be substantial as the average RH for the LB was around 50% for September and 22% for June.

The spectral features in the attenuation coefficients for the two months are almost identical. This is to be expected as the same refractive index was used. The difference in the magnitude of the attenuation coefficients is due primarily to the smaller magnitude of the size distribution for June.

### 4.4.1 Sensitivity to the Coarse Mode Refractive Index

The attenuation coefficients at 0.55, 1.06, 2.5 and 8.5 μm are evaluated for September. The limits of the integral over the radius of the size distribution function are separated into a fine mode part, 0.001 to 1.0 μm and a coarse mode part, 1.001 to 50 μm. Attenuation coefficients for the fine mode and the coarse mode contribution are calculated. For the fine mode calculation the smoke aerosol refractive index (for 1% soot) was used and for the coarse mode, alternatively the 1% soot smoke aerosol refractive index and the Jabiru coarse mode aerosol refractive index were used. The accuracy of the procedure was tested by ensuring that the sum of the two parts was equal to a full calculation over the size range, 0.001 to 50 μm, using the 1% smoke aerosol refractive index. The fine mode part dominates the extinction coefficients at shorter wavelengths (< 1 μm) but for longer wavelengths the coarse mode is the dominant component, in terms of extinction. These results are presented in Table 10.

*Table 10: The percentage of the fine mode aerosol contributing to the extinction coefficient and the difference between the coarse mode and the fine mode as a percentage of the fine mode*

| Part | Wavelength (μm) | | | |
|---|---|---|---|---|
| | 0.55 | 1.06 | 2.5 | 8.5 |
| Fine | 87% of total | 72% of total | 30% of total | 43% of total |
| Coarse | 0.7% diff | 0.7% diff | 27% diff | 49% diff |

The fine mode part is given as a percentage of the total extinction coefficient. The coarse mode part is the difference between the coarse mode part for a 1% soot smoke aerosol refractive index and a Jabiru coarse mode aerosol refractive index calculation of the extinction coefficient. This is given as a percentage of the 1% soot smoke aerosol extinction coefficient. Where the coarse mode part is dominant (thermal wavelengths) the difference is significant (27 and 49 %).

The attenuation coefficients at thermal wavelengths are very small, with extinction coefficients in the order of $10^{-6}\ m^{-1}$ compared with $10^{-5}\ m^{-1}$ for the other wavelengths. Correspondingly the amount of radiation scattering taking place in the thermal wavebands is very small. The error in using the 1% soot smoke aerosol refractive index over the entire size range is significant in percentage terms. This should not affect calculations of atmospheric transmission appreciably since the extinction coefficients upon which atmospheric transmission depends, are small.

## 4.5 Incorporating the Attenuation Coefficients into MODTRAN

Two choices are available: to include an independent Jabiru vertical aerosol profile (vertical aerosol particle number concentration profile) and normalised extinction coefficients or to use the default vertical aerosol profile (using the value of VIS that is obtained from the Jabiru measurements) and include the normalised extinction coefficients for the Jabiru aerosol. In the latter case, the flexible aerosol scheme could be used to translate, scale, stretch and compress the boundary layer profile. The inversion height and the height of the tropopause could then be modelled more accurately. However it is not possible to alter the shape of the profile in the boundary layer, which is assumed to be exponential for VIS $\geq$ 23km. The measurements made around Jabiru showed a profile that was constant with altitude in the lower boundary layer region. The only way to force the profile to follow a constant value below the inversion height is to input a user defined vertical aerosol profile. In this report the default vertical aerosol profile of MODTRAN is used. For higher altitudes the profile is dependent on the season and the volcanic conditions. The spectral parameters are modelled by using the Jabiru size distribution and average particle refractive index and using the default aerosol profile, which is a function of VIS and season, from MODTRAN.

Internal consistency is required between the normalised attenuation coefficients calculated using the stand alone Mie code and the scale factor for the vertical aerosol profile in MODTRAN. This is ensured by using the value of the extinction coefficient at 550 nm (calculated using the Mie code) in the Koschmieder formula to determine the correct VIS to use in MODTRAN.

To execute MODTRAN for the Jabiru aerosol following this procedure, use is made of card 2 (main aerosol and cloud options) to select the aerosol profile and cards 2D, 2D1 and 2D2 as required, for entering the spectral parameters [3]. The Mie code outputs the extinction, scattering, absorption and asymmetry parameters.

The rural aerosol model is selected by setting IHAZE=1 (note the spectral parameters will be overwritten by the user defined parameters), which in turn sets ISEASN. IVULCN=0,1 is

selected for a background stratospheric aerosol profile. The ARUSS = 'USS' option is chosen, which enables user defined aerosol spectral optical property calculations. The values for the attenuation coefficients are then input in card 2D2 with the number of spectral grid points specified on card 2D and the tittle on card 2D1 (Fig.17, Appendix B).

The procedure for incorporating the attenuation coefficients into MODTRAN needs to be checked. A recalculation of the rural aerosol attenuation coefficients of Shettle and Fenn is made using the stand alone Mie code. These are then input into MODTRAN the way it would be done if incorporating user defined spectral parameters (ARUSS = 'USS' option). The results are compared to calculations using the default rural aerosol model. If the procedure has been followed correctly, the answers should be the same or very close, allowing for numerical imprecision. The results of these calculations are presented in Chapter 5.

# 5. Calculation of Atmospheric Transmission

In DSTO, MODTRAN is often used to calculate atmospheric transmission. The atmospheric transmission allows the user to take account of the amount of attenuation of target radiation (and background) due to the atmosphere, at an EO (UV, visible or NIR) or IR sensor.

In the remainder of this report, calculations are made of the atmospheric transmission for a dry season atmosphere based around Jabiru in the N.T.. This is done for a range of paths: horizontal, vertical and slant paths over a series of ranges. The calculations are performed using the Jabiru aerosol attenuation coefficients for the 1% soot smoke aerosol and the 10% soot smoke aerosol, for both June and September. The results are then compared to the results generated by the default models in MODTRAN (rural and maritime). This is done over visible and thermal wavebands.

## 5.1 Checking the Calculations

A MODTRAN run is defined by selecting the U.S. standard 1976 atmosphere and the rural aerosol with VIS = 23 km in the tape5 file. A second MODTRAN run is executed using the default U.S. standard atmosphere of MODTRAN and the default aerosol profile for a VIS = 23 km; then the procedure outlined in Section 4.5 is followed to incorporate Mie calculations of the attenuation coefficients for the rural aerosol model into MODTRAN. The spectral refractive index and the parameters of the bi-modal lognormal size distribution function are taken from the report of Shettle and Fenn. The comparison of the two calculations provides a check of two things: that the spectral attenuation coefficients are calculated correctly using the Mie code and that they are incorporated correctly into MODTRAN.

The size distribution function employed by Shettle and Fenn is given in Section 2.2.1.4 with the parameters of the size distribution given in Table 11.

*Table 11: Parameters of the Rural aerosol model of Shettle and Fenn.*

| Distribution | $N_1$ | $r_1$ | $\sigma_1$ | $N_2$ | $r_2$ | $\sigma_2$ |
|---|---|---|---|---|---|---|
| Rural Vis = 23 km | | | | | | |
| RH=0% | 16230.63 | 0.02700 | 0.35 | 2.03 | 0.4300 | 0.4 |
| RH= 50% | 15 661.76 | 0.02748 | 0.35 | 1.96 | 0.4377 | 0.4 |

The rural aerosol refractive index is a mixture of 70% water soluble and 30% dust-like aerosol. The water soluble component refractive index is given in Table 17 in Appendix A. The dust-like aerosol refractive index is given in the report of Shettle and Fenn [12] and is similar to the modified dust-like aerosol refractive index given in Table 17.

Before proceeding with comparative calculations of the atmospheric transmission, a comparison of the aerosol attenuation coefficients calculated with the Mie code is made: first with those given in the report by Shettle and Fenn then with those given in MODTRAN (extracted from the source code). Shettle and Fenn provide parameters of the size distribution functions for the aerosol models as a function of VIS and RH. The values in Table 11 have been reproduced from their report. They do not provide tables of attenuation coefficients for these exact parameters. Attenuation coefficients are given for the rural aerosol model assuming a total particle number concentration of 15000/cm3 and for a RH of 50%. This value for the number concentration corresponds to a VIS around 23 km. The geometric mean radius and the standard deviation are the same as those given in Table 11. A calculation of spectral attenuation coefficients using this modified value for $N_1$ produces answers that are similar to those reported by Shettle and Fenn. The reason for the difference is not known. It could be that a different or earlier version of the Mie scattering code was used by Shettle and Fenn with different algorithms and levels of precision. The inclusion of the parameters of the size distribution function is straightforward and is not likely to result in error. It is more likely that the source of disagreement between the results is due to the numerical implementation of the Mie algorithms. A check of the sensitivity of the calculation to the values of rmin and rmax was made (adjusting rmin between 0.0001 and 0.01 and rmax between 50 and 100 μm); no significant difference was observed.

The attenuation coefficients calculated using the aerosol models of Shettle and Fenn are listed in MODTRAN for RH of 0, 70, 80 and 99%. Rather than recalculate the attenuation coefficients using the Mie code for the rural aerosol model with one of these values for RH; a comparison is made between the RH=0% attenuation coefficients extracted from the MODTRAN source code with the calculated attenuation coefficients for RH=50%. The difference is small, since the hygroscopic growth in particle size and changes in refractive index are small between 0 and 50% RH. The results are shown in Figure 11. The attenuation coefficients have been normalised by the extinction coefficient at 550 nm. The attenuation coefficients agree to around 2 significant figures.

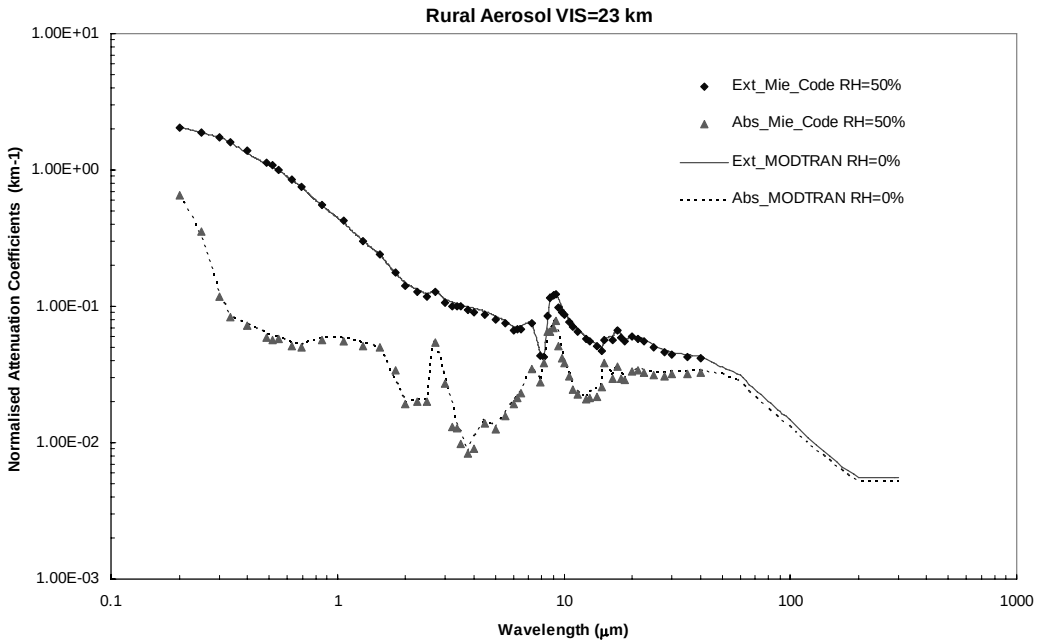


*Figure 11: Normalised aerosol attenuation coefficients for the rural aerosol model. Mie code refers to those calculated using the stand alone Mie code. MODTRAN refers to those extracted from the MODTRAN source code. Ext – extinction and Abs – Absorption.*

The next step is to redo the calculation of attenuation coefficients using the value of $N_1$ given in Table 6. These are the correct attenuation coefficients to be input into MODTRAN for the rural aerosol model.

The results of the two atmospheric transmission calculations were compared over the visible, 3-5 μm and 8-12 μm wavebands. The latter two wavebands can be referred to interchangeably as the mid-wave IR (MWIR) waveband and the long-wave IR (LWIR) waveband. The value of the aerosol extinction coefficient that was calculated at 550 nm was used in the Koschmeider formulae to calculate the surface meteorological range. The result gives a VIS = 21.5 km, which is different to the VIS = 23 km that Shettle and Fenn claim the parameters given in Table 11 should produce. This is most likely due to the fact that only an approximate value for the Rayleigh scattering coefficient of air was used in the Koschmeider formulae.

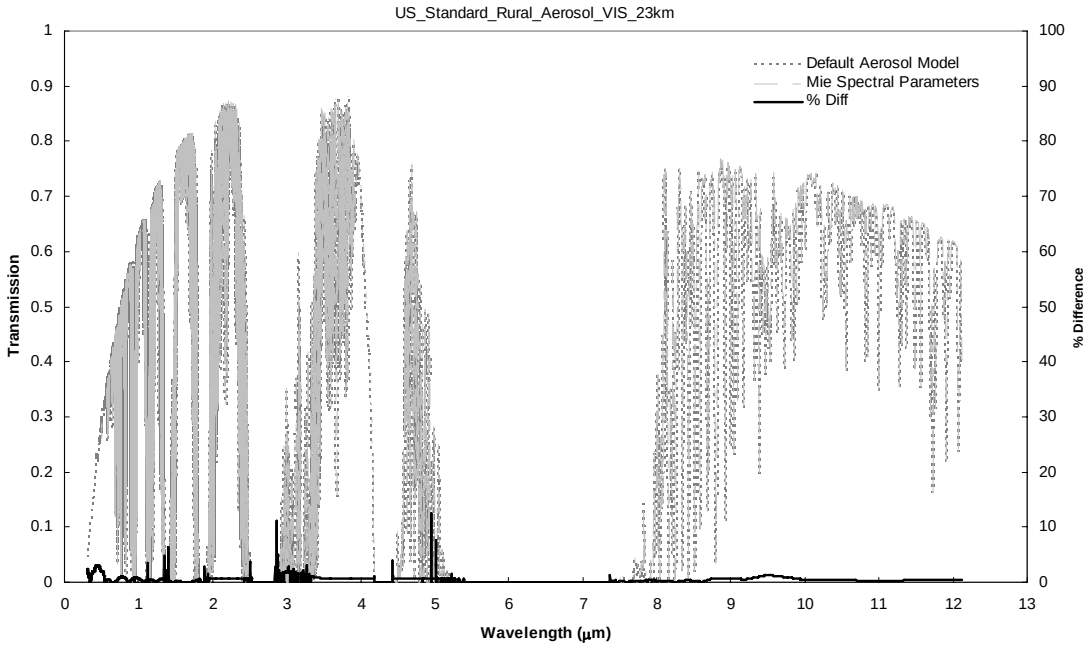


*Figure 12: Atmospheric transmission for the US Standard 1976 model atmosphere for a rural aerosol with VIS = 23 km.*

The Mie spectral parameters graph corresponds to the calculation of transmission using the spectral parameters obtained for the rural aerosol model using the stand alone Mie code. The default aerosol model graph is calculated using the inbuilt rural aerosol model as given in MODTRAN. The % diff is the difference in percentage terms between the two calculations taken with respect to the default aerosol model calculation. The majority of spectral features are the same. They are due primarily to molecular absorption.

The agreement over these wavebands lies within 15% for each spectral point (at a spectral resolution of 5 $cm^{-1}$ FWHM) with a peak difference of 12.5%. The majority of values agree well within 5%. The exceptions are for spectral points that are included in the default aerosol model in MODTRAN but not in the Mie calculations. Another difference is due to the slightly different values for the surface RH. The sea level RH for the US standard 1976 atmosphere is 46%; the spectral parameters that were calculated using the Mie code correspond to a surface RH of 50%. A third difference may be due to any differences in the numerical precision of the two calculations. The parameters stored in MODTRAN were calculated from a separate code. The difference is less than 5% for the majority of wavelengths. We conclude that the spectral parameters are calculated correctly using the Mie code and the inclusion of these parameters into MODTRAN using the ARUSS='USS' option is being done correctly. A difference between transmissions of less that 5% (for the majority of wavelengths) is acceptable, given other uncertainties that enter into the calculations such as the experimental uncertainty in the measured size distributions.

## 5.2 Calculation of Atmospheric Transmission for a Jabiru Smoke Aerosol

### 5.2.1 Jabiru Climate

The top end of the Northern Territory is a tropical environment. It is primarily defined by two main seasons: the dry and the wet. The measurements of the atmospheric aerosol were conducted from an aircraft over Jabiru and surrounding areas of Kakadu National Park and on the ground at ERISS (the Environmental Research Institute of the Supervising Scientist) field station in Jabiru East, opposite Jabiru airport. ERISS is part of the Supervising Scientist Division located within the Australian Government Department of the Environment and Heritage. The measurements were made in the months of June and September; this corresponds to the dry season. The majority of the measurements were undertaken in the afternoon or late morning. In Section 4.3.1 we determined that the Jabiru lower boundary layer aerosol was measured at an average RH of 50% for September and 22% for June. The difference in scattering and extinction coefficients will not be large for RH of 0, 22 and 50%. The model atmosphere used should ideally have a RH profile that has a sea level RH of around 50% or less. The tropical model atmosphere is used, modified by the water vapour profile from the mid-latitude summer (MLS) model.

Jabiru is located around twenty seven metres above sea level. This elevation should not have a major impact on aerosol concentration and hence it is assumed Jabiru is located at sea level. In Table 12 are climate averages for Jabiru airport for the months of June and September over a twenty year period from 1984 to 2004 [47].

*Table 12: Climate averages for Jabiru airport.*

| Climate averages for – JABIRU AIRPORT | June | September |
|---|---|---|
| Mean 9am Air Temp - deg C | 24.4 | 27.2 |
| Mean 9am Relative Humidity - % | 58 | 61 |
| Mean 9am Water Vapour Density – gm/m3 | 12.83 | 15.77 |
| | | |
| Mean 3pm Air Temp - deg C | 31 | 35.4 |
| Mean 3pm Delative Humidity - % | 34 | 26 |
| Mean 3pm Water Vapour Density - gm/m3 | 10.32 | 10.20 |

The 3 pm data is more representative of the typical conditions that were encountered when the aircraft measurements were undertaken. From this information calculations of water vapour density are carried out. From Tables 12 and 13 it is apparent that the MLS model water vapour density profile is a good compromise between the 9 am and 3 pm values for Jabiru (for both months). The Sub-Arctic summer water vapour density is closer to the values measured in September. To keep the number of calculations to a minimum, a single composite atmosphere is selected. In the future the inclusion of the Sub-Artic summer water vapour profile could be considered. A variant of the Clausius-Clapeyron equation [48] is used to determine how the RH will change as the temperature is raised. The initial temperature is $21^{\circ}$ C (MLS model) and the RH is 76%; the final temperature is $26.5^{\circ}$ C (tropical model) giving a RH of 55%. The tropical model with a MLS water vapour profile gives a reasonable approximation to the atmosphere encountered at Jabiru. Importantly the RH on the ground

will be around 50% which is consistent with the average lower boundary layer RH measured during September.

*Table 13: A selection of atmospheric parameters for some of the model atmospheres in MODTRAN.*

| Ground Level Values | Tropical | MLS | US Standard | Sub-Artic Summer |
|---|---|---|---|---|
| Temperature - deg C | 26.5 | 21 | 15 | 14 |
| Relative Humidity - % | 75.5 | 76 | 46 | 75 |
| Water Vapour Density – gm/m3 | 18.97 | 13.98 | 5.89 | 9.09 |

### 5.2.2 Transmission Calculations

Aerosol spectral parameters were calculated using the Mie code and included in atmospheric transmission calculations for a range of paths and over different wavebands. Atmospheric transmission was calculated using the 1% soot smoke aerosol model for June and September. The 1% soot smoke aerosol extinction coefficient at 550 nm for September is 0.0245 $km^{-1}$ which gives a surface meteorological range VIS = 108 km. This value was entered into MODTRAN so that there was consistency between the calculated attenuation coefficients and the vertical scale factor. The value of VIS was obtained using the Koschmeider formulae (Section 2.4). The value used for the Rayleigh scattering coefficient for air at the surface for a wavelength of 550 nm is an approximation. It depends in general on the absolute humidity. The Koscmeider formula applies to scattering coefficients measured at the surface. The extinction coefficients calculated using the Mie code were obtained using average size distribution data from the lower boundary layer. They do not include measurements on the ground. This is part of the reason why the values for VIS are large. The scattering coefficient on the ground is unlikely to differ by much from the average boundary layer value. The large VIS is a reflection of the very low aerosol loading in the region around Jabiru.

For June the extinction coefficient at 550 nm is 0.0114 $km^{-1}$ corresponding to a VIS = 170 km. The smoky region aerosol extinction coefficient at 550 nm is 0.0197 $km^{-1}$ which gives a VIS = 125 km. These parameters are summarised in Table 14.

*Table 14: This table contains parameters for the two smoke models for both June and September. Estimated observer visibility is obtained using the approximate expression given.*

| Aerosol Model | Month | Scatt Coeff @ 550 nm $km^{-1}$ | Surface Meteorological Range VIS $km$ | Observer Visibility (est.) $V_{obs} \approx VIS/(1.3\pm0.3)$ $km$ |
|---|---|---|---|---|
| 1% Soot Smoke | June | 0.0114 | 170 | 106-170 |
| 1% Soot Smoke | Smoky Region | 0.0197 | 125 | 78-125 |
| 1% Soot Smoke | September | 0.0245 | 108 | 68-108 |
| 10% Soot Smoke | June | 0.0124 | 163 | 102-163 |
| 10% Soot Smoke | September | 0.0273 | 100 | 63-100 |

The smoky region aerosol has less impact on scattering than the average September aerosol. The asymmetry parameter (the integral of the phase function over cosine theta) is the same for

June and September since the same value of the refractive index is used. A calculation involving the default rural and maritime aerosol models of Shettle and Fenn is included for comparison. A range of atmospheric paths are chosen. These are given in Table 15.

*Table 15: The different paths through the atmosphere used in calculations of atmospheric transmission.*

| Profile | Initial Altitude (H1) km | Final Altitude (H2) km | Initial Zenith Angle (at H1) degs. | Range km |
|---|---|---|---|---|
| Horizontal | | | | |
| 1 | 0.05 | 0.05 | | 10 |
| 2 | 1 | 1 | | 10 |
| 3 | 5 | 5 | | 10 |
| Vertical to Ground | | | | |
| 4 | 5 | 0 | 180 | 5 |
| 5 | 10 | 0 | 180 | 10 |
| 6 | 50 | 0 | 180 | 50 |
| Slant to Ground | | | | |
| 7 | 0.05 | 0 | 91 | 2.90 |
| 8 | 1 | 0 | 100 | 5.77 |
| 9 | 1 | 0 | 135 | 1.41 |
| 10 | 5 | 0 | 100 | 29.12 |
| 11 | 5 | 0 | 135 | 7.07 |
| 12 | 10 | 0 | 100 | 58.96 |

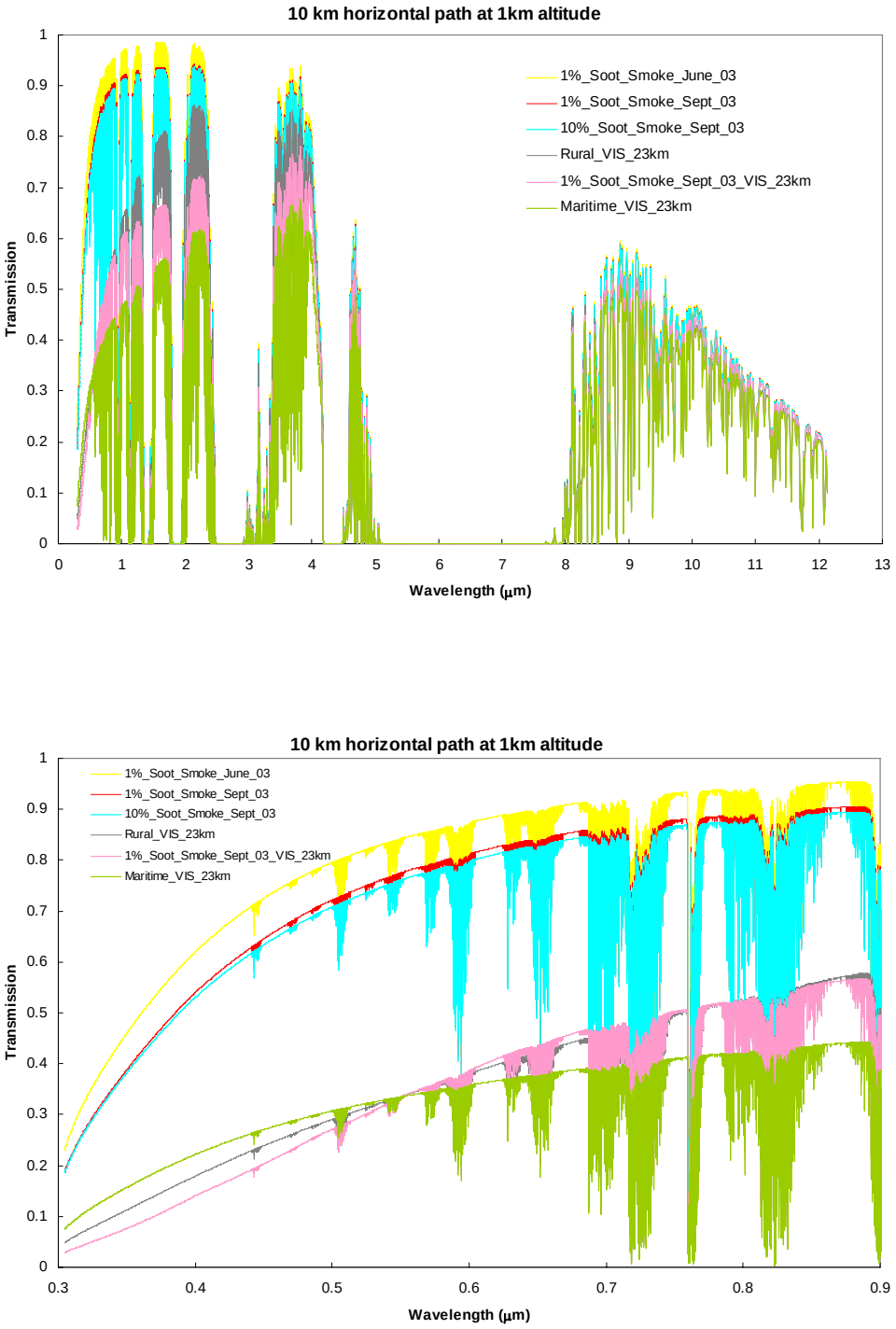


*Figure 13: Atmospheric transmission for a 10 km horizontal path through the atmosphere. Results are also given for the default aerosol models, rural and maritime and for September assuming a VIS=23 km. The second plot shows the same transmission calculations but over the UV, visible and near IR wavelengths only.*

It is apparent from these results that the percentage of soot the smoke is composed of has a minimal impact on the atmospheric transmission. The same is true for June. The 1% soot smoke aerosol model is chosen for the remainder of the transmission calculations. The difference between the Jabiru aerosol and the default MODTRAN models, rural and maritime, is quite large in percentage terms over visible and MWIR wavebands. The water vapour dominates attenuation in the LWIR waveband where the impact of aerosol scattering is less important. The difference between the default model calculations could be due to RH growth effects; particularly for the maritime model due to the fact the coarse mode sea salt is very hygroscopic. The rural model has a coarse mode composed of dust, which is less hygroscopic. The rural and maritime aerosol model calculations assume a VIS = 23 km; the difference between the two calculations will be primarily a result of the different chemical composition of the particles. This difference manifests itself in the refractive index and in the shape of the size distribution. The difference over visible and MWIR wavelengths between the two default model calculations is quite large. To ensure the results are correct a careful check of the MODTRAN runs was made. An independent calculation of the atmospheric transmission for the maritime aerosol model was made using PcModWin 4v1r1 [49]; the identical version to the version of MODTRAN used. The results were the same.

The main conclusion from these results is that due to the small aerosol concentration aloft in this region of the top end of the N.T., there is very little scattering of visible and IR radiation. This is despite the abundance of biomass fires. The viewing conditions whilst on the aircraft were in general very good and the visibility predicted by the Mie calculations agrees well with observation. A smoke haze is clearly visible out towards the horizon but this is 10's of km away. The fires burn out reasonably quickly; new ones will be started but not necessarily at the same location. The distribution of fires is over a relatively large area and with the addition of clean maritime air this will tend to disperse the smoke. In summary, based on our average measurements over one week in June and one week in September 2003 the atmospheric Jabiru aerosol (biomass smoke) will not have a major impact on EO and IR sensor performance. The majority of smoke that impacted on the aircraft measurements was from fires in Arnhem Land (to the East of Jabiru). Fires in other regions of the top end such as south west of Darwin would have had very little impact on the aircraft measurements. The weather patterns (south easterly winds for example) are typical for the region around Jabiru and hence we believe these measurements will be representative of the conditions in general.

This is supported by the measurements made by Gras et al. [50] around Katherine, N.T. in 1997. The fires were located in a lightly wooded savannah area approximately 100 km from Katherine. They found that typical scattering coefficients at a wavelength of 550 nm away from the fires was around $4-5\times10^{-5}\ m^{-1}$ compared with our value for September of around $2.5\times10^{-5}\ m^{-1}$ (Table 9). The observations they made are similar to ours, in that although the boundary layer showed widespread evidence of smoke (e.g. haze), the scattering coefficients away from fires were relatively small. As an aside, it is worth mentioning that they conclude that there are significant differences found between the savannah fire smoke in Northern Australia and the smoke observed in Kalimantan, Borneo Indonesia. Aerosol scattering coefficients in the Indonesian smoke plumes and regionally were larger than those measured in Northern Australia savannah fires. The hygroscopic growth of scattering between 20% and 80% relative humidity was considerably larger for the Indonesian smoke aerosol. Limited

aerosol light absorption data indicated relatively small absorption in the Indonesian smoke. The different combustion phases can explain some of the differences observed between the two regions. In the case of Australian savannah fires there was mixed flaming with smouldering whilst for the Indonesia fires it was predominately smouldering. These and other measurements indicate that underground peat combustion may have had a significant contribution to the Indonesian smoke.

The concentration of particles for the Jabiru measurements is low, leading to scattering coefficients that correspond to large VIS (> 100 km); hence any changes to the aerosol properties are not likely to manifest themselves in calculations of atmospheric transmission. The exception might be if the VIS was unusually high. In this case differences such as those between the rural and maritime models start to manifest themselves in transmission calculations. A calculation of the 1% soot smoke aerosol atmospheric transmission was done for September assuming a 23 km surface meteorological range. This highlights the impact a change in the number concentration has on the results; setting VIS = 23 km artificially scales the vertical profile of aerosol attenuation and we see the effect of this in Figure 13.

The atmospheric transmission in the boundary layer is sensitive to the choice of aerosol model over visible and MWIR wavebands. The effect in the LWIR waveband is minimal. The degree to which the choice of aerosol model impacts on EO and IR sensor performance will depend on whether the range at which the sensors are operating is approaching their detection limit. In this case, gains or losses in transmission, depending on the choice of aerosol model, will be important.

The difference between the band-averaged atmospheric transmission calculations using the Jabiru measurements and the default maritime aerosol model, for averages over visible, MWIR and LWIR wavebands, are summarized in Table 16. This is done for the predicted transmission for September (VIS = 108 km) and for the modified calculation assuming a 23 km VIS.

*Table 16: Differences between the Jabiru aerosol and the rural and maritime models of MODTRAN. These are given as averages over the respective wavebands.*

| Waveband | A - 1% Soot Smoke Sept 03 – VIS=108 km | B - 1% Soot Smoke Sept 03 – scaled VIS=23 km | C - Rural VIS=23 km | D - Maritime VIS =23 km | % Diff A-D | % Diff B-D |
|---|---|---|---|---|---|---|
| Visible | 0.75197 | 0.32652 | 0.33266 | 0.32701 | 130 | 0.15 |
| 3-5 μm | 0.27873 | 0.23679 | 0.25961 | 0.20508 | 36 | 15 |
| 8-12 μm | 0.31107 | 0.29253 | 0.28636 | 0.27797 | 12 | 5 |

The transmission over the 8-12 μm waveband is greater than the 3-5 μm waveband due to the averaging done over the wavebands. The 3-5 μm band is effectively divided into two separate sub bands with transmission dropping to zero around 4.3 μm. It is not suggested that band averaging should be used in general (particularly over the 3-5 μm waveband). It is employed here solely to illustrate some points. The sensitivity of the transmission to the VIS is significant over the visible waveband. It diminishes over the IR wavebands. When using the default aerosol models it is important to have knowledge of the surface meteorological range so that proper account can be taken of the aerosol concentration versus altitude. The difference between the predicted atmospheric transmission for September versus that obtained assuming a VIS = 23 km is significant over the visible waveband. The difference between the maritime model and the Jabiru aerosol for September with a VIS = 23 km is primarily due to the different chemical composition of the aerosol, manifesting itself in a different spectral refractive index. It is also due to differences in the shape of the size distribution function. The identical vertical aerosol profile has been used for the two calculations.

In Figures 14-16 the numbers in the legends refer to the paths given in Table 15. The transmission calculations over paths 1, 2 and 3 were done for the 1% soot smoke aerosol for both June and September.

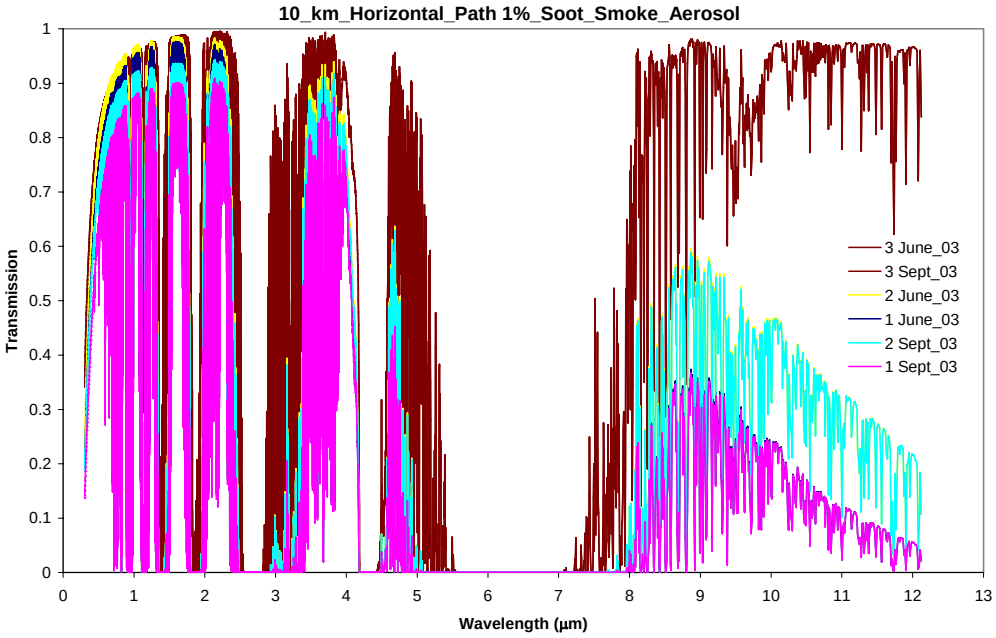


*Figure 14: Atmospheric transmission for a series of 10 km horizontal paths. The numbers in the legend correspond to the paths given in Table 15.*

The transmission is the same for June and September for the 5 km altitude horizontal path (profile 3) since this passes through the free troposphere and not the boundary layer.

The relative difference between June and September is the same over different paths and hence for the remainder of the transmission graphs for profiles 4 through 12, we only include results from September. The purpose of choosing the slant paths is to highlight how the transmission will change compared with horizontal paths. This can be illustrated with the results from September alone.

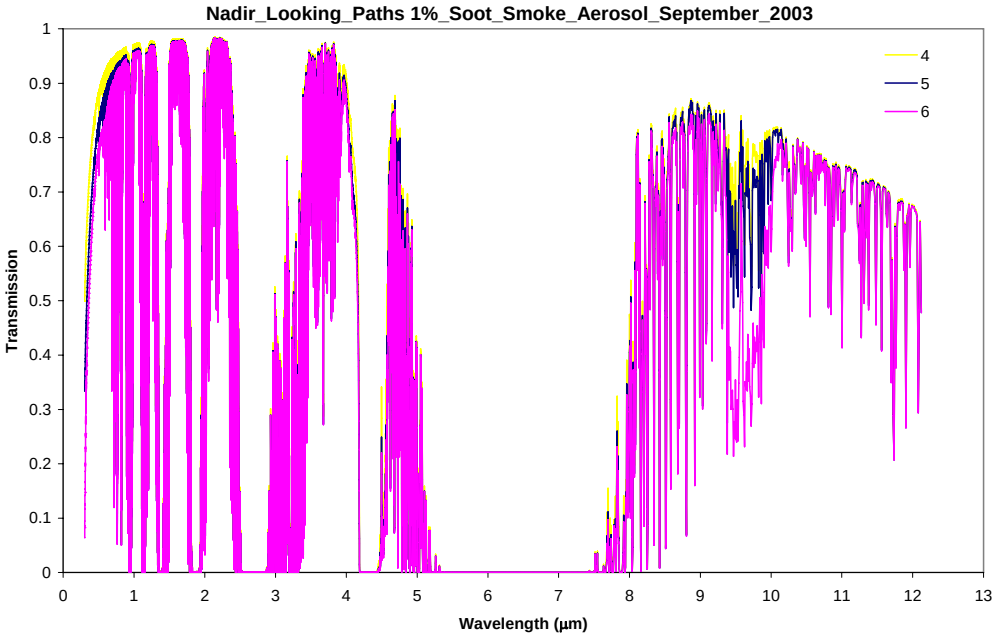


*Figure 15: Atmospheric transmission for a series of Nadir looking paths. The numbers in the legend correspond with the paths given in Table 15.*

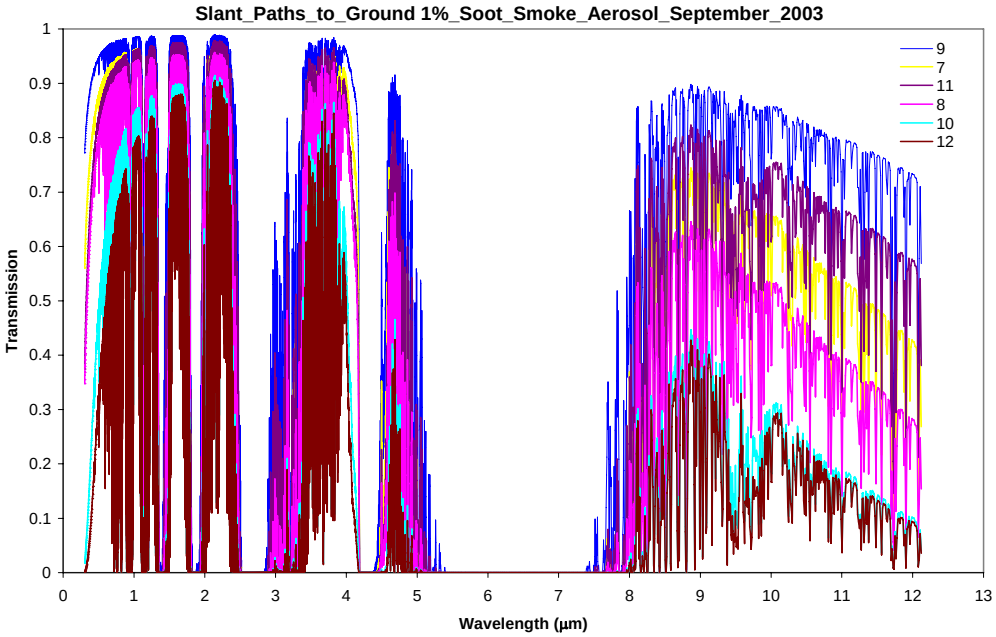


*Figure 16: Atmospheric transmission for a series of Slant paths. The numbers in the legend correspond with the paths given in Table 15.*

Figures 14-16 serve to highlight how the transmission can change over different paths through the atmosphere. The effect of aerosol extinction is most notable over the visible and MWIR wavebands. The LWIR waveband highlights the impact water vapour has on transmission of IR radiation. The aerosol extinction has the biggest impact over longer path lengths, for example the slant path from 10 km to the ground at a Zenith angle of $100^{\circ}$. There are less significant differences between the transmissions over the same horizontal path length at different altitudes. For the Nadir looking paths the differences are insignificant, which is to be expected as all three paths pass through the same region of the boundary layer. Overall the results show the type of behaviour that could be reasonably expected. The main conclusion is that for the Jabiru 1% soot smoke aerosol the effect on transmission is small other then for very long path lengths such as profile 12.

# 6. Conclusions

This report presents a quantitative assessment of the transmission of radiation through the atmosphere in the tropical North of Australia. The assessment is based on aircraft measurements of the aerosol size distribution and chemical composition that were conducted during June and September 2003. This has enabled a comparison of the difference between using a default aerosol model in MODTRAN and the measured Jabiru aerosol that was incorporated into MODTRAN. A number of the measurements used in this report were obtained on an aircraft; thereby allowing a probe of the vertical dimension. This data provides information on how the aerosol behaves at ground level and throughout the boundary layer and the free troposphere. The data used in this report is a combination of these aircraft measurements and ground based chemistry measurements and analysis. This is a more fundamental set of experimental data than atmospheric transmission measurements on the ground over arbitrary paths. This improves our ability to use MODTRAN effectively but also for the first time DSTO has a deeper understanding of the aerosol behaviour in terms of the microphysics, chemistry and optical properties. Transmission measurements are valuable but on their own do not constitute a complete scientific study of the aerosol properties needed to validate and understand the aerosol models in MODTRAN. The summary of the results of the atmospheric transmission calculations are given in Section 5.2.2.

In the next section we summarise some issues that need further investigation and additional work that may be carried out in the future.

## 6.1 Issues and Future Work

DSTO is conducting ongoing ground based measurements of the aerosol light scattering coefficient at Jabiru. The three wavelength nephelometer has been installed at ERISS and has been operating since September 2004. Analysis of the scattering coefficients will enable long term trends in the aerosol loading in the region to be determined. This includes the months of June and September. Additionally, differences between the wet and dry season aerosol loading will be determined. This data can be used in combination with the results presented in this report to enable a comprehensive understanding of the aerosol behaviour in the region

around Jabiru. The nephelometer will be operated to at least September 2006. The data will be analysed and a report produced.

No attempt was made to model the RH dependence of the Jabiru smoke aerosol. This can be done in the future using the procedure outlined in the report by Shettle and Fenn [5], for example. This involves taking into account particle diameter growth and also changes in the refractive index of the particles. The default vertical aerosol profile of MODTRAN was used rather than the user supplied vertical aerosol profile. Data is available on the aerosol size distribution in the boundary layer (BL) and the free troposphere (FT). This data could be incorporated into MODTRAN to more accurately represent the vertical aerosol changes, particularly at the inversion. Above 20 000 feet (6.1 km), which is the limit of the aircraft measurements, it is necessary to revert to the use of the default aerosol profile (certainly for the stratosphere and upper atmosphere). This is unlikely to alter the results appreciably since the attenuation coefficients in the boundary layer are very small, giving rise to a large VIS. The only difference will be in the height of the inversion layer (BL-FT transition altitude) which differs between June and September. Hence for a horizontal path that is above the inversion height in June but below it in September, the atmospheric transmission may change appreciably (in percentage terms) but still remain small overall.

The Jabiru smoke aerosol refractive index was used in calculations of the spectral efficiency factors over the entire size range (fine and coarse modes). This is not very accurate for the thermal wavebands. The amount of radiation scattering due to aerosols in these wavebands is relatively small and the impact on atmospheric transmission is not likely to be significant. In the future the Mie scattering code could be modified to treat the refractive index of each mode separately. This would require a further investment of time that is not warranted for these initial calculations. Alternatively use could be made of a single Jabiru composite aerosol particle. This is the approach adopted by Shettle and Fenn.

Another approach is to treat the aerosol as an external mixture. The attenuation coefficients of each component are calculated and then combined as a volume weighted average to determine a total attenuation coefficient. This type of aerosol mixture may be more representative of the aerosol near a smoke plume.

In future work the lower and upper boundary layer size distributions could be averaged together to produce a single boundary layer size distribution. For September the height of the lower boundary layer region was often larger than the default altitude of the boundary layer region in MODTRAN. In June they were similar. This is not likely to alter the results presented here appreciably. The vertical aerosol profile shape would change and show a more exponential decrease with altitude, due to the inclusion of the upper boundary layer size distribution. This is consistent with the default aerosol profile for VIS $\geq$ 23 km in the boundary layer aerosol models of MODTRAN. The majority of the issues discussed here would become more important if the aerosol loading around Jabiru was much higher. The relatively clean conditions and the small impact on the scattering of radiation means that there is little value in assessing the differences in aspects of the aerosol model that are likely to have little impact on atmospheric transmission. Finally the measurements of the absorption coefficient at 530 nm could be included in Figures 9 and 10, following some further post processing of the data, as was done with the measured scattering coefficients.

The average refractive index was obtained from averages over components with the percentages given by the mass fraction of each component primarily derived from MOUDI measurements on the ground at Jabiru. No attempt was made to perform a APCA or a CMB receptor model study such as carried out by Maenhaut et al. However as discussed in Section 3.3.1 the results are not inconsistent with the analysis of Maenhaut et al. In the future a more accurate determination of the aerosol source components contributing to the regional aerosol could be made. For the fine mode in the dry season the biomass smoke will be the dominant component. Any improvements in the determination of biomass burning aerosol refractive index from the region around Jabiru would be welcomed and should be used to recalculate the quantities given in this report. The data of Sutherland and Khana are the only data that we are aware of that is likely to be close to the type of data expected from the analysis of biomass burning smoke.

### 6.1.1 Developing a Jabiru Aerosol Model

Another possible application of the data presented in this report is to use it to determine a more general smoke aerosol model. This type of model would be similar to the boundary layer aerosol models of Shettle and Fenn. One approach would be to attempt to separate the background aerosol component in the region from the smoke aerosol. This is similar to how Shettle and Fenn model urban aerosols; a rural background with a soot component to take account of aerosols of an anthropogenic origin.

A similar approach could be taken with the Jabiru aerosol. The background is likely to contain the same or similar components to the rural model of Shettle and Fenn. Fresh and aged smoke aerosol components could then be combined with the rural background component to produce aerosol models with a low and high residual soot component. It may also be necessary to use the Maritime model as the background component due to the proximity of the coastline (Jabiru is around 60 km from the coast). Additional modification of the vertical profile to take account of the inversion height and layering of the smoke near the top of the boundary layer is also necessary. This was observed on more than one occasion during the aircraft measurements. This may have a larger impact on atmospheric transmission calculations for an airborne sensor above the boundary layer over long slant ranges.

# 7. Acknowledgements

The author would like to thank Dr Bill Cornette for general discussions about the atmospheric aerosol pertaining to the results presented in this report. His suggestions about improving the vertical aerosol profile and how to go about producing a Jabiru aerosol model were valuable. In particular the author would like to thank Dr Cornette for providing the aerosol attenuation coefficients that were extracted from the MODTRAN source code. He also provided the detailed information about MOSART; in particular where it offered improvements over MODTRAN.

# 8. References


1. Long Range Research (LRR) Force Research Area (FRA) Plan 2005-06 – 2007-08 Ver: 5 (7th June 2005). By authority of Corporate Leader LRR FRA, DSTO, Edinburgh
2. Carr S. B., Gras J. L., Hackett M. T. and Keywood M. D. (2005), *Aerosol Characterisation in the Northern Territory of Australia during the Dry Season with an Emphasis on Biomass Burning*, DSTO Research Report DSTO-RR-0298
3. Kneizys, F. X. et al. (1995) *The MODTRAN 2/3 and LOWTRAN 7 Model*, Ontar Corporation, North Andover MA
4. Berk, A. et al. (2004) *MODTRAN5 Version 2 Revision 3 USER'S MANUAL,* SPECTRAL SCIENCES, INC, Burlington MA and Air force Geophysics Laboratory, Hanscom AFB, MA
5. Berk, A. et al. (1999) *MODTRAN4 USER'S MANUAL,* Air force Geophysics Laboratory, Hanscom AFB, MA
6. Kneizys, F. X. et al. (1983) *Atmospheric Transmittance/Radiance: Computer Code LOWTRAN 6* , Air force Geophysics Laboratory AFGL-TR-83-0187, Hanscom AFB, MA
7. Findlay, G. A. and Cutten, D. R. (1989) *Transmission of Infrared Radiation through the Australian Atmosphere: Predictions using the LOWTRAN Model,* DSTO Surveillance Research Laboratory Technical Report SRL-0031-TR
8. Cutten, D. R. (1985) *Atmospheric IR Transmission Measurements in a Tropical Maritime Environment: Comparison with the LOWTRAN 6 Model,* DSTO Electronics Research Laboratory Technical Memorandum ERL-0331-TM
9. Cutten, D. R. (1983) *Atmospheric IR Transmission Data for a Temperate Maritime Environment,* DSTO Electronics Research Laboratory Technical Report ERL-0265-TR
10. Cutten, D. R. (1979) *Preliminary Assessment of Infra-red Transmission Data Measured Over 'Ocean-Type' Waters in a Temperate Environment,* DSTO Electronics Research Laboratory Technical Memorandum ERL-0063-TM
11. Gambling, D. J. (1972) *An Aerosol Attenuation Model for the Visible and Infrared Spectral Regions,* Weapons Research Establishment Technical Note WRE-Technical Note-593 (AP)
12. Cutten D. R. (1972) *A Review of Atmospheric Scattering in the Visible Spectral Region,* Weapons Research Establishment Technical Note WRE-Technical Note-788 (AP)
13. Cornette, W. M. and Acharya P. K. (1995) *Moderate Spectral Atmospheric Radiance and Transmittance Program (MOSART). Volume I: Installation Reference Manual. Volume II: Users' Reference Manual; Volume III: Technical Reference Manual; Volume IV: Software Reference Manual*, U.S. Air Force Phillips Laboratory, Hanscom Air Force Base, Massachusetts, PL-TR-94-2244
14. Shettle, E. P. and Fenn, R. W. (1979) *Models for the Aerosols of the Lower Atmosphere and the Effects of Humidity Variations on Their Optical Properties,* Air Force Geophysics Laboratory Technical Report AFG-TR-79-0214
15. Shettle, E. P. and Fenn, R. W. (1976) *Models of the Atmospheric Aerosols and their Optical Properties*, in AGARD Conference Proceedings No. 183 Optical Propagation in the Atmosphere AGARD-CP-183, available from the U.S. National Technical Information Service, AD A028-615

16. Gathman, S. G. and Davidson, K. L. (1993) *The Navy Oceanic Vertical Aerosol Model,* Naval Command, Control and Ocean Surveillance Center RDT&E Division, Technical Report 1634
17. Mie, G. (1908) Beitrage zur Optik truber Medien, speziell kolloidaler Metallosungen, *Ann. Phys. Leipzig*, **25** 377-445
18. Bohren, C. F. and Huffman, D. R. (1998) *Absorption and Scattering of Light by Small Particles* , Wiley Science Paperback Series Edition, John Wiley and Sons, New York, Chapter 4
19. Anderson, G. P. et al. (1997) *Addition of NOVAM (Navy Oceanic Vertical Aerosol Models) to MODTRAN in Support of OMPS,* PL/Geophysics Directorate, Hanscom AFB, MA
20. Kim, Y. P., Seinfeld, J. H and Saxena, P (1993) Atmospheric gas-aerosol equilibrium 1. Thermodynamic model, *Aerosol Science and Technology*, **19** 157-181
21. Sutherland, R. A. and Khanna, R. K. (1991) Optical Properties of Organic-based Aerosols Produced by Burning Vegetation, *Aerosol Science and Technology*, **14** 331-342
22. Trentmann, J. et al. (2002) Simulation of a biomass-burning plume: Comparison of model results with observations, *J. Geophys. Res.,* **107** (D2) AAC 5-1 - AAC 5-15
23. Rothman, L. S. et al. (2003) The HITRAN molecular spectroscopic database: edition of 2000 including updates through 2001, *Journal of Quantitative Spectroscopy & Radiative Transfer*, **82** 5–44
24. Toon, O. B. et al. (1976) The Optical Constants of Several Atmospheric Aerosol Species: Ammonium Sulfate, Aluminum Oxide and Sodium Chloride*, J. Geophys. Res.,* **81** (33) 5733-5748
25. Grant, K. E. et al. (1999) Modeling the spectral optical properties of ammonium sulfate and biomass burning aerosols: parameterization of relative humidity effects and model results, *Atmospheric Environment,* **33** 2603-2620
26. Maxwell-Garnett, J. C. (1904) Colors in metal glasses and in metallic films, *Phil. Trans. Roy. Soc. London*, **203** 2014-2020.
27. Sano, I. and Sonoyo, M. (1998) Polarimetic Properties of Aerosol Particles, *Earth Planets Space,* **50** 513-519
28. Schuster, G. L. (2004) *Inferring the Specific Absorption and Concentration of Black Carbon from Aeronet Aerosol Retrievals*, PhD Thesis, Pennsylvania State University
29. Erlick, C., (2005) Effective refractive indices of water and sulfate drops containing absorbing inclusions, *J. Atmos. Sci.*, in press, 2005.
30. Chylek, P. et al. (1988) Scattering of electromagnetic waves by composite spherical particles: experiment and effective medium approximations, *Applied Optics,* **27** (12) 2396-2404
31. Lesins, P. et al. (2002) A study of internal and external mixing scenarios and its effect on aerosol optical properties and direct radiative forcing, *J. Geophys. Res.,* **107** (D10) AAC 5-1 – AAC 5-12
32. Levoni, C. et al. (1997) Atmospheric aerosol optical properties: a database of radiative characteristics for different components and classes, *Applied Optics,* **36** (30) 8031-8041
33. Maenhaut, W. et al. (2000) Aerosol Composition at Jabiru, Australia, and Impact of Biomass Burning, *J. Aerosol Sci.,* **31** (Suppl. 1) S745-S746
34. Volz, F. E. (1972) Infrared absorption by atmospheric aerosol substances, *J. Geophys. Res.,* **77** 1017-1031
35. Volz, F. E. (1973) Infrared optical constants ammonium sulfate, Sahara dust, volcanic pumace and flyash, *Applied Optics,* **12** 564-568

36. Volz, F. E. (1972) Infrared refractive index of atmospheric substance, *Applied Optics*, **11** 755-759
37. d'Almeida, G. A. et al. (1991) *Atmospheric Aerosols Global Climatology and Radiation Characteristics*, A. Deepak Publishing, Hampton, Va., USA
38. Grams, G. W. et al. (1974) Complex index of refraction of airborne soil particles, *Journal of Applied Meteorology*, **13** 459-471
39. Patterson, E. M. et al. (1977) Commonalities in measured size distributions for aerosols having a soil derived component, *Journal of Geophysical Research*, **82** 2074-2082
40. Highwood, E. J. et al. (2003) Radiative properties and direct effect of Saharan dust measured by the C-130 aircraft during Saharan Dust Experiment (SHADE): 2. Terrestrial spectrum, *Journal of geophysical Research*, **108** (D18) SAH 5-1 – SAH 5-13
41. World Climate Program, WCP-112 (1986) *A preliminary cloudless standard atmosphere for radiation computation,* WMO/TD-No. 24, World Meteorological Organisation, Geneva
42. Haywood, J. et al. (2003) Radiative properties and direct radiative effect of Saharan dust measured by the C-130 aircraft during SHADE: 1. Solar spectrum, *Journal of geophysical Research*, **108** (D18) SAH 4-1 – SAH 4-16
43. Myhre, G. et al. (2003) Modeling the radiative impact of mineral dust during the Saharan Dust Experiment (SHADE) campaign, *Journal of geophysical Research*, **108** (D18) SAH 6-1 – SAH 6-13
44. Fouquart, Y. et al. (1987) Observations of Saharan Aerosols: Results of ECLATS Field Experiment. Part II: Broadband Radiative Characteristics of the Aerosols and Vertical Radiative Flux Divergence, *Journal of Climate and Applied Meteorology,* **26** 38-52
45. Chandler, J.P. (1972), A program for efficient integration of rate equations and least-squares fitting of chemical reaction data, *Computers and Biomedical Research,* **5** 515-534
46. Wiscombe, W. J. (1996), *MIEV Documentation*, NASA Goddard Space Flight Center, Greenbelt, MD
47. Climate Averages for Australian Sites (2005) *Averages for Jabiru Airport,* Commonwealth Bureau of Meteorology, Australia
48. see e.g. Seinfeld, J. H. and Pandis, S. N. (1998) *Atmospheric Chemistry and Physics: From Air Pollution to Climate Change*, John Wiley and Sons, New York
49. Ontar Corporation (2002) *PcModWin Manual Version 4.0 v1r1 Version 1.1*, Ontar Corporation, North Andover, MA
50. Gras, J. L. et al. (1999) Some Optical Properties of Smoke Aerosol in Indonesia and Tropical Australia, *Geophys. Res. Letters,* **26** (10) 1393-1396

# Appendix A: Aerosol Spectral Refractive Indices

*Table 17: The real (n) and imaginary (k) parts of the aerosol component spectral refractive indices: m= n + i k.*

| Wavelength Microns | Water Soluble | | Sea Salt | | Modified Dust-Like | | Elemental Carbon | | Organic Carbon | |
|---|---|---|---|---|---|---|---|---|---|---|
| | n | k | n | k | n | k | n | k | n | k |
| 0.200 | 1.530 | 0.070 | 1.510 | 1.00E-04 | 1.530 | 0.0700 | 1.500 | 0.350 | 1.550 | 0.00E+00 |
| 0.250 | 1.530 | 0.030 | 1.510 | 5.00E-06 | 1.530 | 0.0300 | 1.620 | 0.450 | 1.550 | 0.00E+00 |
| 0.300 | 1.530 | 0.008 | 1.510 | 2.00E-06 | 1.530 | 0.0015 | 1.740 | 0.470 | 1.550 | 0.00E+00 |
| 0.337 | 1.530 | 0.005 | 1.510 | 4.00E-07 | 1.530 | 0.0015 | 1.750 | 0.470 | 1.550 | 0.00E+00 |
| 0.400 | 1.530 | 0.005 | 1.500 | 3.00E-08 | 1.530 | 0.0015 | 1.750 | 0.460 | 1.550 | 0.00E+00 |
| 0.488 | 1.530 | 0.005 | 1.500 | 2.00E-08 | 1.530 | 0.0015 | 1.750 | 0.450 | 1.550 | 0.00E+00 |
| 0.515 | 1.530 | 0.005 | 1.500 | 1.00E-08 | 1.530 | 0.0015 | 1.750 | 0.450 | 1.550 | 0.00E+00 |
| 0.550 | 1.530 | 0.006 | 1.500 | 1.00E-08 | 1.530 | 0.0015 | 1.750 | 0.440 | 1.550 | 0.00E+00 |
| 0.633 | 1.530 | 0.006 | 1.490 | 2.00E-08 | 1.530 | 0.0015 | 1.750 | 0.430 | 1.550 | 0.00E+00 |
| 0.694 | 1.530 | 0.007 | 1.490 | 1.00E-07 | 1.530 | 0.0015 | 1.750 | 0.430 | 1.550 | 0.00E+00 |
| 0.860 | 1.520 | 0.012 | 1.480 | 3.00E-06 | 1.520 | 0.0015 | 1.750 | 0.430 | 1.550 | 0.00E+00 |
| 1.060 | 1.520 | 0.017 | 1.470 | 2.00E-04 | 1.520 | 0.0015 | 1.750 | 0.440 | 1.507 | 1.27E-06 |
| 1.300 | 1.510 | 0.020 | 1.470 | 4.00E-04 | 1.460 | 0.0015 | 1.760 | 0.450 | 1.496 | 1.36E-05 |
| 1.536 | 1.510 | 0.023 | 1.460 | 6.00E-04 | 1.400 | 0.0015 | 1.770 | 0.460 | 1.489 | 3.90E-05 |
| 1.800 | 1.460 | 0.017 | 1.450 | 8.00E-04 | 1.330 | 0.0015 | 1.790 | 0.480 | 1.480 | 7.60E-05 |
| 2.000 | 1.420 | 0.008 | 1.450 | 1.00E-03 | 1.260 | 0.0015 | 1.800 | 0.490 | 1.470 | 0.00E+00 |
| 2.250 | 1.420 | 0.010 | 1.440 | 2.00E-03 | 1.220 | 0.0090 | 1.810 | 0.500 | 1.463 | 8.68E-05 |
| 2.500 | 1.420 | 0.012 | 1.430 | 4.00E-03 | 1.180 | 0.0090 | 1.820 | 0.510 | 1.449 | 2.53E-04 |
| 2.700 | 1.400 | 0.055 | 1.400 | 7.00E-03 | 1.180 | 0.0130 | 1.830 | 0.520 | 1.425 | 5.64E-04 |
| 3.000 | 1.420 | 0.022 | 1.610 | 1.00E-02 | 1.160 | 0.0120 | 1.840 | 0.540 | 1.415 | 1.03E-01 |
| 3.200 | 1.430 | 0.008 | 1.490 | 3.00E-03 | 1.220 | 0.0100 | 1.860 | 0.540 | 1.482 | 1.01E-01 |
| 3.392 | 1.430 | 0.007 | 1.480 | 2.00E-03 | 1.260 | 0.0130 | 1.870 | 0.550 | 1.484 | 1.09E-01 |
| 3.500 | 1.450 | 0.005 | 1.480 | 1.60E-03 | 1.280 | 0.0110 | 1.880 | 0.560 | 1.529 | 8.80E-02 |
| 3.750 | 1.452 | 0.004 | 1.470 | 1.40E-03 | 1.270 | 0.0110 | 1.900 | 0.570 | 1.519 | 4.30E-02 |
| 4.000 | 1.455 | 0.005 | 1.480 | 1.40E-03 | 1.260 | 0.0120 | 1.920 | 0.580 | 1.511 | 2.80E-02 |
| 4.500 | 1.460 | 0.013 | 1.490 | 1.40E-03 | 1.260 | 0.0140 | 1.940 | 0.590 | 1.482 | 7.42E-03 |
| 5.000 | 1.450 | 0.012 | 1.470 | 2.50E-03 | 1.250 | 0.0160 | 1.970 | 0.600 | 1.441 | 7.65E-04 |
| 5.500 | 1.440 | 0.018 | 1.420 | 3.60E-03 | 1.220 | 0.0210 | 1.990 | 0.610 | 1.333 | 5.69E-03 |
| 6.000 | 1.410 | 0.023 | 1.410 | 1.10E-02 | 1.150 | 0.0370 | 2.020 | 0.620 | 1.426 | 2.21E-01 |
| 6.200 | 1.430 | 0.027 | 1.600 | 2.20E-02 | 1.140 | 0.0390 | 2.030 | 0.625 | 1.470 | 2.12E-01 |
| 6.500 | 1.460 | 0.033 | 1.460 | 5.00E-03 | 1.130 | 0.0420 | 2.040 | 0.630 | 1.504 | 1.49E-01 |
| 7.200 | 1.400 | 0.070 | 1.420 | 7.00E-03 | 1.400 | 0.0550 | 2.060 | 0.650 | 1.532 | 2.17E-01 |
| 7.900 | 1.200 | 0.065 | 1.400 | 1.30E-02 | 1.150 | 0.0400 | 2.120 | 0.670 | 1.543 | 1.90E-01 |
| 8.200 | 1.010 | 0.100 | 1.420 | 2.00E-02 | 1.130 | 0.0740 | 2.130 | 0.680 | 1.580 | 2.12E-01 |
| 8.500 | 1.300 | 0.215 | 1.480 | 2.60E-02 | 1.300 | 0.0900 | 2.150 | 0.690 | 1.610 | 1.86E-01 |
| 8.700 | 2.400 | 0.290 | 1.600 | 3.00E-02 | 1.400 | 0.1000 | 2.160 | 0.690 | 1.588 | 1.72E-01 |
| 9.000 | 2.560 | 0.370 | 1.650 | 2.80E-02 | 1.700 | 0.1400 | 2.170 | 0.700 | 1.621 | 2.35E-01 |
| 9.200 | 2.200 | 0.420 | 1.610 | 2.60E-02 | 1.720 | 0.1500 | 2.180 | 0.700 | 1.685 | 2.22E-01 |
| 9.500 | 1.950 | 0.160 | 1.580 | 1.80E-02 | 1.730 | 0.1620 | 2.190 | 0.710 | 1.711 | 1.91E-01 |

| | | | | | | | | | | |
|---|---|---|---|---|---|---|---|---|---|---|
| 9.800 | 1.870 | 0.095 | 1.560 | 1.60E-02 | 1.740 | 0.1620 | 2.200 | 0.715 | 1.757 | 1.39E-01 |
| 10.000 | 1.820 | 0.090 | 1.540 | 1.50E-02 | 1.750 | 0.1620 | 2.210 | 0.720 | 1.752 | 9.60E-02 |
| 10.591 | 1.760 | 0.070 | 1.500 | 1.40E-02 | 1.620 | 0.1200 | 2.220 | 0.730 | 1.716 | 2.90E-02 |
| 11.000 | 1.720 | 0.050 | 1.480 | 1.40E-02 | 1.620 | 0.1050 | 2.230 | 0.730 | 1.689 | 6.44E-03 |
| 11.500 | 1.670 | 0.047 | 1.480 | 1.40E-02 | 1.590 | 0.1000 | 2.240 | 0.740 | 1.657 | 0.00E+00 |
| 12.500 | 1.620 | 0.053 | 1.420 | 1.60E-02 | 1.510 | 0.0900 | 2.270 | 0.750 | 1.627 | 0.00E+00 |
| 13.000 | 1.620 | 0.055 | 1.410 | 1.80E-02 | 1.470 | 0.1000 | 2.280 | 0.760 | 1.614 | 9.27E-03 |
| 14.000 | 1.560 | 0.073 | 1.410 | 2.30E-02 | 1.520 | 0.0850 | 2.310 | 0.775 | 1.619 | 0.00E+00 |
| 14.800 | 1.440 | 0.100 | 1.430 | 3.00E-02 | 1.570 | 0.1000 | 2.330 | 0.790 | 1.609 | 0.00E+00 |
| 15.000 | 1.420 | 0.200 | 1.450 | 3.50E-02 | 1.570 | 0.1000 | 2.330 | 0.790 | 1.607 | 0.00E+00 |
| 16.400 | 1.750 | 0.160 | 1.560 | 9.00E-02 | 1.600 | 0.1000 | 2.360 | 0.810 | 1.607 | 5.88E-03 |
| 17.200 | 2.080 | 0.240 | 1.740 | 1.20E-01 | 1.630 | 0.1000 | 2.380 | 0.820 | 1.605 | 0.00E+00 |
| 18.000 | 1.980 | 0.180 | 1.780 | 1.30E-01 | 1.640 | 0.1150 | 2.400 | 0.825 | 1.599 | 0.00E+00 |
| 18.500 | 1.850 | 0.170 | 1.770 | 1.35E-01 | 1.640 | 0.1200 | 2.410 | 0.830 | 1.599 | 0.00E+00 |
| 20.000 | 2.120 | 0.220 | 1.760 | 1.52E-01 | 1.680 | 0.2200 | 2.450 | 0.850 | 1.690 | 2.00E-02 |
| 21.300 | 2.060 | 0.230 | 1.760 | 1.65E-01 | 1.770 | 0.2800 | 2.460 | 0.860 | 1.646 | 2.50E-02 |
| 22.500 | 2.000 | 0.240 | 1.760 | 1.80E-01 | 1.900 | 0.2800 | 2.480 | 0.870 | 1.612 | 3.20E-02 |
| 25.000 | 1.880 | 0.280 | 1.760 | 2.05E-01 | 1.970 | 0.2400 | 2.510 | 0.890 | 1.550 | 5.00E-02 |
| 27.900 | 1.840 | 0.290 | 1.770 | 2.75E-01 | 1.890 | 0.3200 | 2.540 | 0.910 | 1.454 | 8.70E-02 |
| 30.000 | 1.820 | 0.300 | 1.770 | 3.00E-01 | 1.800 | 0.4200 | 2.570 | 0.930 | 1.337 | 1.83E-01 |
| 35.000 | 1.920 | 0.400 | 1.760 | 5.00E-01 | 1.900 | 0.5000 | 2.630 | 0.970 | 1.199 | 6.35E-01 |
| 40.000 | 1.860 | 0.500 | 1.740 | 1.00E+00 | 2.100 | 0.6000 | 2.690 | 1.000 | 2.140 | 1.12E+00 |

# Appendix B: Example Mie2new and MODTRAN 4 v1 r1 Input Files

```
1    0    0
1    1    0    0  Cal. of spectral attenuation coeffs for Smoke particles
  1.0       8.0       2.0       20.0     2.0
   60.      2.        120.       2.
0.001        50.     1000.   599    1         4  Sum of 3 lognormals for Sept 03.
340.0              0.051    0.241
884.0              0.066    0.190
1.75              0.605    0.207
     0.550        1.548           4.8E-3
```

*Figure 16: Example mie2new input file (mie2new.tp5). This is for the 1% soot smoke aerosol refractive index at 550 nm and the size distribution for September 2003.*

```
M   1    1    0    0    0    2    0    0    0    0    0    0    0   0.000   0.00
     T   5   365.000
    1    0USS 0    0    0    0   108.000     0.000     0.000     0.000     0.000
   61    0    0    0
  0.000e+00 1% Soot Smoke Sept 03 VIS 108km RH approx 50%
   .20 3.0486 .26255 .7605   .25 2.6895 .16296 .7138   .30 2.2689 .54371 .6800
   .34 2.0050 .08936 .6728   .40 1.6015 .07375 .6649   .49 1.1978 .06010 .6557
   .52 1.1038 .05691 .6524   .55 1.0000 .05349 .6495   .63 .81241 .04562 .6412
   .69 .71818 .04176 .6360   .86 .56872 .03556 .6286  1.06 .48617 .02971 .6179
  1.30 .45098 .02499 .6214  1.54 .42353 .02180 .6305  1.80 .38534 .01783 .6648
  2.00 .35002 .01464 .7008  2.25 .31012 .01432 .7213  2.50 .26717 .01356 .7407
  2.70 .22806 .01719 .7725  3.00 .25125 .12077 .7658  3.20 .25560 .11235 .7431
  3.39 .24419 .11281 .7384  3.50 .24269 .09385 .7239  3.75 .19894 .05099 .7280
  4.00 .17017 .03396 .7323  4.50 .12093 .01409 .7414  5.00 .08277 .00721 .7496
  5.50 .04711 .00986 .7650  6.00 .15108 .11631 .7932  6.20 .14572 .10721 .7881
  6.50 .11666 .07796 .7793  7.20 .12840 .09537 .7662  7.90 .10041 .07481 .8531
  8.20 .10402 .07905 .8711  8.50 .09821 .07146 .7867  8.70 .09435 .06530 .5834
  9.00 .11104 .08130 .5563  9.20 .10606 .07543 .5988  9.50 .08967 .06042 .6113
  9.80 .07565 .04573 .6111 10.00 .06140 .03255 .6155 10.59 .03660 .01317 .6276
 11.00 .02628 .00635 .6265 11.50 .02024 .00432 .6381 12.50 .01480 .00391 .6555
 13.00 .01505 .00598 .6591 14.00 .01102 .00386 .6655 14.80 .00973 .00404 .6877
 15.00 .01062 .00525 .6877 16.40 .00994 .00576 .6133 17.20 .00917 .00536 .5586
 18.00 .00810 .00495 .5643 18.50 .00760 .00481 .5834 20.00 .01024 .00760 .5380
 21.30 .01016 .00825 .5358 22.50 .01033 .00889 .5309 25.00 .01087 .01004 .5301
 27.90 .01459 .01416 .5235 30.00 .02292 .02267 .5154 35.00 .06064 .06032 .4717
 40.00 .04506 .04445 .4371
     1.000                          10.000
   833.000 50000.000     1.000     5.000TM        W1
    0
```

*Figure 17: Example MODTRAN input (tape 5) file. This is for the 1% soot smoke aerosol refractive index and size distribution for September 2003 for a 10 km path at a 1 km altitude. The model atmosphere is tropical with a MLS water vapour profile.*

# Appendix C: The Mie2new Source Code Header

```
PROGRAM MIE2NEW
cc    PROGRAM MIE2 (INPUT,OUTPUT,TAPE5,TAPE6,TAPE8)
C
C     ****************************************************************
C
C     MIE SCATTERING ANALYSIS
C
C     AIR FORCE GEOPHYSICS LABORATORY
C     BASED ON A PROGRAM DEVELOPED BY RRA FT WORTH, TEXAS
C
C     REVISED BY:  E. SHETTLE, J. CHETWYND, L. ABREU
C                  OPTICAL PHYSICS DIVISION, AFGL, HANSCOM AFB, MA 01731
C                  D. LONGTIN
C                  OPTIMETRICS, INC. BURLINGTON, MA 01803
C
C     REVISED 10-97 BY MICHAEL W. MATTHEW (mwm-ssi)
C                      SPECTRAL SCIENCES, INC.
C                      BURLINGTON, MA 01803
C
C     *****************  CONTROL CARDS ARE AS FOLLOWS  ***************
C
C     1   NNPROB,INTEG,ISEE                          FORMAT(3I5)
C     2   IPROB,KPROB,IUNITS,IDB,XX(L), L=1,20       FORMAT(4I5,20A4)
C     3   DTHET1,CHANG1,DTHET2,CHANG2,DTHET3         FORMAT(9F10.2)
C               ,CHANG3,DTHET4,CHANG4,DTHET5
C     4   RMIN,RMAX,ZAPRXS,NSTEP,IRADSP,MOM,NEQ,NEQL FORMAT(3E10.3,4I5,
C                                                        A20)
C     5A  RI(I),ENR(I), #CARDS = NSTEP+1             FORMAT(2E15.5)
C     5B  D,ALPHA,B,GAMMA                            FORMAT(4E15.8)
C     5C  CONST,RPMAX,D,ALPHA                        FORMAT(4E15.8)
C     5D1 ANUM1,R1,SIG1                              FORMAT(3E15.8)
C     5D2 ANUM2,R2,SIG2                              FORMAT(3E15.8)
C     5E1 ANUM1,R1,SIG1                              FORMAT(3E15.8)
C     5E2 ANUM2,R2,SIG2                              FORMAT(3E15.8)
C     5E3 ANUM3,R3,SIG3                              FORMAT(3E15.8)
C     5F  RAIN                                       FORMAT(1E15.8)
C     5G  RAIN,ZN,B,C,D                              FORMAT(5E15.8)
C     6   PM (COMPLEX),WAVEL,PML                     FORMAT(3E15.8,A20)
C
C     ****************************************************************
C
C     CARD 1
C     NNPROB:  NUMBER OF PROBLEMS HAVING DIFFERENT SIZE DISTRIBUTIONS.
C              REPEAT CARDS 2-6 FOR EACH PROBLEM
C     INTEG:   THE TRAPEZODIAL RULE WILL BE USED TO INTEGRATE THE PHASE
C              FUNCTION WHEN INTEG <= 0
C     ISEE:    PRINT OPTION PARAMETER.  IF ISEE >0, THE MICROSCOPIC
C              MIE DATA FOR EACH SIZE PARAMETER ARE PRINTED. NORMALLY
C              SET ISEE TO 0 AND PRINT ONLY FOR CHECK OUT
C
C     CARD 2
C     IPROB:   PROBLEM IDENTIFICATION NUMBER
C     KPROB:   NUMBER OF WAVELENGTHS OR INDICES OF REFRACTION IN THE
C              PROBLEM. REPEAT CARD #6 FOR EACH VALUE.
C     IUNITS:  UNITS GOVERNING THE SIZE DISTRIBUTION PARAMETERS AND
C              WAVELENGTHS ON CARDS 4-6. FLAG CONTROLS THE LABELS TO BE
C              PRINTED WITH OUTPUT
C              IMPORTANT: THE PARAMETERS ON CARDS 4-6 MUST BE INPUTTED
C              USING INTERNALLY CONSISTENT UNITS
C              0 = MICROMETERS
C              1 = MILLIMETERS
C     IDB:     FLAG TO CONVERT THE SCATTERING DATA TO DB/KM
C              0 = NO
C              1 = YES
C     XX:      IDENTIFYING NAME OR LABEL, PRINTED WITH OUTPUT
```

```
C
C     CARD 3
C     DTHET:   STEP SIZE WITHIN FIRST ANGLE INTERVAL (IN DEGREES)
C     CHANG1:  UPPER LIMIT OF FIRST ANGLE INTERVAL (IN DEGREES)
C     DTHET2:  STEP SIZE WITHIN SECOND ANGLE INTERVAL (IN DEGREES)
C     CHANG2:  UPPER LIMIT OF SECOND ANGLE INTERVAL (IN DEGREES)
C     DTHET3:  STEP SIZE WITHIN THIRD ANGLE INTERVAL (IN DEGREES)
C              NOTE: THE TOTAL NUMBER OF ANGLES <= 150
C
c      new   1997
c
C     CHANG3:  UPPER LIMIT OF THIRD ANGLE INTERVAL (IN DEGREES)
C     DTHET4:  STEP SIZE WITHIN 4th ANGLE INTERVAL (IN DEGREES)
c
C     CHANG4:  UPPER LIMIT OF    5th  ANGLE INTERVAL (IN DEGREES)
C     DTHET5:  STEP SIZE WITHIN  6th  ANGLE INTERVAL (IN DEGREES)
c
C     CARD 4
C     RMIN:    THE MINIMUM RADIUS WHERE THE AEROSOL SIZE DISTRIBUTION
C              IS DEFINED
C     RMAX:    THE MAXIMUM RADIUS WHERE THE AEROSOL SIZE DISTRIBUTION
C              IS DEFINED
C     ZAPRXS:  LOWERMOST SIZE PARAMETER WHERE THE NW APPROXIMATIONS ARE
C              USED FOR QEX, QABS AND G, AND RAY OPTICS FOR THE PHASE
C              MATRIX ELEMENTS
C              NOTE: ZAPRXS SHOULD BE GREATER THAN 500
C     NSTEP:   THE NUMBER OF STEPS TO BE USED WHEN INTEGRATING OVER THE
C              AEROSOL SIZE DISTRIBUTION, NSTEP <= 799
C              NSTEP = (# OF DIFFERENT RADII) - 1
C     IRADSP:  FLAG THAT INDICATES THE TYPE OF RADII SPACING TO BE USED
C              WHEN INTEGRATING OVER THE AEROSOL SIZE DISTRIBUTION
C               0 = RADII READ FROM CARDS (MUST SET NEQ = 0)
C               1 = ARITHMETICALLY SPACED INTEGRATION INTERVALS
C               2 = RADII UNIFORMLY SPACED IN N(R)*R**MOM
C     MOM:     MOMENT OF THE SIZE DISTRIBUTION, N(R)*R**MOM
C              (ONLY USED WHEN IRADSP = 2)
C     NEQ:     METHOD OF DEFINING THE AEROSOL SIZE DISTRIBUTION
C               0 = THE PARTICLE RADII AND THE CORRESPONDING SIZE
C                   DISTRIBUTION ARE READ FROM CARDS
C               1 = MODIFIED GAMMA DISTRIBUTION
C               2 = TRUNCATED POWER LAW
C               3 = SUM OF 2 LOG NORMAL DISTRIBUTIONS
C               4 = SUM OF 3 LOG NORMAL DISTRIBUTIONS
C               5 = MARSHALL-PALMER RAINDROP DISTRIBUTION
C               6 = GENERALIZED EXPONENTIAL RAINDROP DISTRIBUTION
C     NEQL:    IDENTIFYING NAME OR LABEL FOR SIZE DISTRIBUTION
C
C     CARD 5
C
C     NOTE THAT CARD 5 IS READ IN SUBROUTINE SIZES AND DEPENDING ON NEQ,
C     MAY INVOLVE MORE THAN ONE DATA CARD
C
C     CARD 5A, USER DEFINED DISTRIBUTION (NEQ = 0)
C     RI(I):   AEROSOL SIZE RADIUS
C     ENR(I):  CORRESPONDING SIZE DISTRIBUTION VALUE (= DN(R)/DR)
C     NOTE THAT #CARDS MUST EQUAL (NSTEP + 1)
C
C     CARD 5B, MODIFIED GAMMA SIZE DISTRIBUTION (NEQ = 1)
C     INPUT PARAMETERS: D,ALPHA,B,GAMMA
C     N(R)  =  D*(R**ALPHA)*EXP(-B*R**GAMMA)
C
C     CARD 5C, TRUNCATED POWER LAW (NEQ = 2)
C     INPUT PARAMETERS: CONST,RPMAX,D,ALPHA
C     N(R)  =  CONST,     R <= RPMAX
C     N(R)  =  D*R*ALPHA, R >  RPMAX
C
C     CARDS 5D1 AND 5D2, SUM OF 2 LOG NORMAL DISTRIBUTIONS (NEQ = 3)
C     INPUT PARAMETERS: ANUM1,R1,SIG1
C                       ANUM2,R2,SIG2
C     MUST HAVE BOTH CARDS!
C     DN(R)/DLOGR = ANUM1/(SIG1*SQR(2*PI))*EXP(-(LOG(R/R1)/(2*SIG1))**2)
```

```
C                 +ANUM2/(SIG2*SQR(2*PI))*EXP(-(LOG(R/R2)/(2*SIG2))**2)
C
C     CARDS 5E1 - 5E3, SUM OF 3 LOG NORMAL DISTRIBUTIONS (NEQ = 4)
C     INPUT PARAMETERS: ANUM1,R1,SIG1
C                       ANUM2,R2,SIG2
C                       ANUM3,R3,SIG3
C     MUST HAVE THREE CARDS!
C
C     CARD 5F, MARSHALL-PALMER RAINDROP DISTRIBUTION (NEQ = 5)
C     INPUT PARAMETER: RAIN (RAINRATE IN MM/HR)
C     N(R)  =  2*8000*EXP(-4.1*(RAIN**-0.21)*2*R)
C
C     CARD 5G, GENERALIZED EXPONENTIAL RAINDROP DISTRIBUTION (NEQ = 6)
C     INPUT PARAMETERS: RAIN, ZN, B, C, D
C     N(R)  =  (2*ZN*(RAIN**B))*EXP(-C*(RAIN**D)*2*R)
C
C     CARD 6,  # OF DATA CARDS EQUALS KPROB
C     WAVEL:   WAVELENGTH
C     PM:      COMPLEX INDEX OF REFRACTION, REAL PART
C              AND IMAGINARY PART. THE IMAGINARY PART
C              SHOULD BE NEGATIVE, BUT POSITIVE VALUES ARE INTERNALLY
C              SET TO NEGATIVE
C     PML:     IDENTIFYING NAME OR LABEL FOR INDEX OF REFRACTION
C
C     ****************************************************************
C
```

*Figure 18: This is the Mie2new Fortran source code header for the main program. It is taken from the program in the mie directory that is distributed with MODTRAN.*

DISTRIBUTION LIST

The Aerosol Models in MODTRAN: Incorporating Selected Measurements from Northern Australia

S. B. Carr

**AUSTRALIA**

| **DEFENCE ORGANISATION** | **No. of copies** |
|---|---|
| **Task Sponsor** | |
| CISRD | 1 Printed |
| **S&T Program** | |
| Chief Defence Scientist | 1 |
| Deputy Chief Defence Scientist Policy | 1 |
| AS Science Corporate Management | 1 |
| Director General Science Policy Development | 1 |
| Counsellor Defence Science, London | Doc Data Sheet |
| Counsellor Defence Science, Washington | Doc Data Sheet |
| Scientific Adviser to MRDC, Thailand | Doc Data Sheet |
| Scientific Adviser Joint | 1 |
| Navy Scientific Adviser | Doc Data Sht & Dist List |
| Scientific Adviser – Army | 1 |
| Air Force Scientific Adviser | 1 |
| Scientific Adviser to the DMO | Doc Data Sht & Dist List |
| **Information Sciences Laboratory** | |
| Chief of Intelligence, Surveillance and Reconnaissance Division | Doc Data Sht & Dist List |
| Chief of Electronic Warfare and Radar Division | Doc Data Sht & Dist List |
| Chief of Weapon Systems Division | Doc Data Sht & Dist List |
| Research Leader Imagery Systems Branch | Doc Data Sht & Dist List |
| Research Leader Electro-Optic Electronic Warfare Branch | Doc Data Sht & Dist List |
| Head IEOS Group | 1 |
| S. B. Carr | 5 Printed |

| | |
|---|---|
| **DSTO Library and Archives** | |
| Library Edinburgh | 2 Printed |
| Defence Archives | 1 Printed |
| | |
| **Capability Development Group** | |
| Director General Maritime Development | Doc Data Sheet |
| Director General Land Development | 1 |
| Director General Capability and Plans | Doc Data Sheet |
| Assistant Secretary Investment Analysis | Doc Data Sheet |
| Director Capability Plans and Programming | Doc Data Sheet |
| | |
| **Chief Information Officer Group** | |
| Director General Australian Defence Simulation Office | Doc Data Sheet |
| AS Information Strategy and Futures | Doc Data Sheet |
| Director General Information Services | Doc Data Sheet |
| | |
| **Strategy Group** | |
| Director General Military Strategy | Doc Data Sheet |
| Assistant Secretary Governance and Counter-Proliferation | Doc Data Sheet |
| | |
| **Navy** | |
| **Maritime Operational Analysis Centre, Building 89/90 Garden Island Sydney NSW**<br>Deputy Director (Operations)<br>Deputy Director (Analysis) | Doc Data Sht & Dist List |
| Director General Navy Capability, Performance and Plans, Navy Headquarters | Doc Data Sheet |
| Director General Navy Strategic Policy and Futures, Navy Headquarters | Doc Data Sheet |
| | |
| **Air Force** | |
| SO (Science) - Headquarters Air Combat Group, RAAF Base, Williamtown NSW 2314 | Doc Data Sht & Exec Summary |
| | |
| **Army** | |
| **ABCA National Standardisation Officer**<br>Land Warfare Development Sector, Puckapunyal | e-mailed Doc Data Sheet |
| SO (Science) - Land Headquarters (LHQ), Victoria Barracks NSW | Doc Data & Exec Summary |
| SO (Science), Deployable Joint Force Headquarters (DJFHQ) (L), Enoggera QLD | Doc Data Sheet |
| | |
| **Joint Operations Command** | |
| Director General Joint Operations | Doc Data Sheet |
| Chief of Staff Headquarters Joint Operations Command | Doc Data Sheet |
| Commandant ADF Warfare Centre | Doc Data Sheet |
| Director General Strategic Logistics | Doc Data Sheet |
| COS Australian Defence College | Doc Data Sheet |

**Intelligence and Security Group**

| | |
|---|---|
| AS Concepts, Capability and Resources | 1 |
| DGSTA , Defence Intelligence Organisation | 1 Printed |
| Manager, Information Centre, Defence Intelligence Organisation | 1 |
| Director Advanced Capabilities | Doc Data Sheet |

**Defence Materiel Organisation**

| | |
|---|---|
| Deputy CEO | Doc Data Sheet |
| Head Aerospace Systems Division | Doc Data Sheet |
| Head Maritime Systems Division | Doc Data Sheet |
| Program Manager Air Warfare Destroyer | Doc Data Sheet |
| CDR Joint Logistics Command | |
| Guided Weapon & Explosive Ordnance Branch (GWEO) | Doc Data Sheet |

**OTHER ORGANISATIONS**

| | |
|---|---|
| National Library of Australia | 1 |
| NASA (Canberra) | 1 |
| Library of New South Wales | 1 |

**UNIVERSITIES AND COLLEGES**

**Australian Defence Force Academy**

| | |
|---|---|
| Library | 1 |
| Head of Aerospace and Mechanical Engineering | 1 |
| Hargrave Library, Monash University | Doc Data Sheet |

**OUTSIDE AUSTRALIA**

**INTERNATIONAL DEFENCE INFORMATION CENTRES**

| | |
|---|---|
| US Defense Technical Information Center | 1 |
| UK Dstl Knowledge Services | 1 |
| Canada Defence Research Directorate R&D Knowledge & Information Management (DRDKIM) | 1 |
| NZ Defence Information Centre | 1 |

**ABSTRACTING AND INFORMATION ORGANISATIONS**

| | |
|---|---|
| Library, Chemical Abstracts Reference Service | 1 |
| Engineering Societies Library, US | 1 |
| Materials Information, Cambridge Scientific Abstracts, US | 1 |
| Documents Librarian, The Center for Research Libraries, US | 1 |

| | |
|---|---|
| SPARES | 3 Printed |

**Total number of copies: 37 Printed:13 PDF:24**

**DEFENCE SCIENCE AND TECHNOLOGY ORGANISATION**
**DOCUMENT CONTROL DATA**

1. PRIVACY MARKING/CAVEAT (OF DOCUMENT)

2. TITLE

The Aerosol Models in MODTRAN: Incorporating Selected Measurements from Northern Australia

3. SECURITY CLASSIFICATION (FOR UNCLASSIFIED REPORTS THAT ARE LIMITED RELEASE USE (L) NEXT TO DOCUMENT CLASSIFICATION)

| | |
|---|---|
| Document | (U) |
| Title | (U) |
| Abstract | (U) |

4. AUTHOR(S)

S.B. Carr

5. CORPORATE AUTHOR

Defence Science and Technology Organisation
PO Box 1500
Edinburgh South Australia 5111 Australia

| 6a. DSTO NUMBER | 6b. AR NUMBER | 6c. TYPE OF REPORT | 7. DOCUMENT DATE |
|---|---|---|---|
| DSTO-TR-1803 | AR-013-545 | Technical Report | December 2005 |

| 8. FILE NUMBER | 9. TASK NUMBER | 10. TASK SPONSOR | 11. NO. OF PAGES | 12. NO. OF REFERENCES |
|---|---|---|---|---|
| 2005/1095519 | LRR 04/175 | CISRD | 57 | 50 |

13. URL on the World Wide Web

http://www.dsto.defence.gov.au/corporate/reports/DSTO-TR-1803.pdf

14. RELEASE AUTHORITY

Chief, Intelligence, Surveillance and Reconnaissance Division

15. SECONDARY RELEASE STATEMENT OF THIS DOCUMENT

*Approved for public release*

OVERSEAS ENQUIRIES OUTSIDE STATED LIMITATIONS SHOULD BE REFERRED THROUGH DOCUMENT EXCHANGE, PO BOX 1500, EDINBURGH, SA 5111

16. DELIBERATE ANNOUNCEMENT

No Limitations

17. CITATION IN OTHER DOCUMENTS Yes

18. DEFTEST DESCRIPTORS

Atmospheric propagation, Atmospheric conditions, Aerosols, Electro optical sensors, Northern Australia

19. ABSTRACT

The aerosol models in MODTRAN are discussed. The focus in this report is on the boundary layer aerosol. The second part of the report outlines the major results of aircraft measurements of atmospheric aerosol obtained around Jabiru, N.T., in June and September 2003. These measurements are used to obtain theoretical multimode size distribution functions. The chemistry composition measurements are used with selected results from the literature to derive spectral refractive indices for the biomass burning smoke aerosol. These results are then used in Mie scattering calculations of the aerosol extinction and scattering coefficients. The attenuation coefficients are then incorporated into MODTRAN and compared with the default aerosol models. Finally the Jabiru aerosol is used in calculations of atmospheric transmission over a series of paths: horizontal, vertical and slant paths. The major result is that the aerosol concentration is quite low giving rise to large visibilities and hence the effect of the atmospheric aerosol on the transmission of radiation over visible and thermal wavebands is small for paths less than around 30 km.